


RESEARCH ARTICLE



Assessing the bioactivity of crystalline silica in heated high-temperature insulation wools

Matthew S. P. Boyles^a, David Brown^a, Jilly Knox^b, Michael Horobin^b, Mark R. Miller^c , Helinor J. Johnston^a and Vicki Stone^a

^aNano Safety Research Group, School of Engineering and Physical Sciences, Institute of Biological Chemistry, Biophysics and Bioengineering, Heriot-Watt University, Edinburgh, UK; ^bMorgan Advanced Materials, Thermal Ceramics, Bromborough, UK; ^cCentre for Cardiovascular Science, University of Edinburgh, Edinburgh, UK

ABSTRACT

High-Temperature Insulation Wools (HTIW), such as alumino silicate wools (Refractory Ceramic Fibers) and Alkaline Earth Silicate wools, are used in high-temperature industries for thermal insulation. These materials have an amorphous glass-like structure. In some applications, exposure to high temperatures causes devitrification resulting in the formation of crystalline species including crystalline silica. The formation of this potentially carcinogenic material raises safety concerns regarding after-use handling and disposal. This study aims to determine whether cristobalite formed in HTIW is bioactive *in vitro*. Mouse macrophage (J774A.1) and human alveolar epithelial (A549) cell lines were exposed to pristine HTIW of different compositions, and corresponding heat-treated samples. Cell death, cytokine release, and reactive oxygen species (ROS) formation were assessed in both cell types. Cell responses to aluminium lactate-coated fibers were assessed to determine if responses were caused by crystalline silica. DQ12 α -quartz was used as positive control, and TiO₂ as negative control. HTIW did not induce cell death or intracellular ROS, and their ability to induce pro-inflammatory mediator release was low. In contrast, DQ12 induced cytotoxicity, a strong pro-inflammatory response and ROS generation. The modest pro-inflammatory mediator responses of HTIW did not always coincide with the formation of cristobalite in heated fibers; therefore, we cannot confirm that devitrification of HTIW results in bioactive cristobalite *in vitro*. In conclusion, the biological responses to HTIW observed were not attributable to a single physicochemical characteristic; instead, a combination of physicochemical characteristics (cristobalite content, fiber chemistry, dimensions and material solubility) appear to contribute to induction of cellular responses.

ARTICLE HISTORY

Received 16 November 2017
Revised 7 August 2018
Accepted 15 August 2018

KEYWORDS



Man-made vitreous fibers; DQ12 quartz; pro-inflammatory response; crystalline silica; alkaline earth silicate; AES wools; high-temperature insulation wools; devitrified; *in vitro* toxicology; solubility


Introduction

High-temperature insulation wools (HTIW) used for thermal insulation include alumino silicate wools (ASW; or “Refractory Ceramic Fibers” (RCF)) and alkaline earth silicate (AES) wools. While RCF has been used since the 1950s, AES are relatively new and have been developed to have reduced biopersistence, to decrease their potential hazard to human health. Although epidemiological studies cannot presently rule out the risk of RCF-induced disease (Walker et al., 2002), data derived from human subjects suggest that there is a low risk of lung cancer or mesothelioma (Boffetta et al., 2014; Chiazze et al., 1997), with no overall association with lung cancer-related mortalities (Walker et al., 2002). However, data from animal studies led to the classification of RCF as a Group 2B “possibly carcinogenic to humans” material (IARC, 2002). Accordingly, to reduce the potential risk to workers in high-temperature wool industries, RCF have been replaced by AES wools

(commercially available since 1991) in a number of applications (IARC, 2002). The use of AES is growing globally and accounts for an increasing proportion of total HTIW used by industry. As of 2012, AES production was about 20,000 tons per year for the European market, equal to the market size of RCF (Brown and Harrison 2012).

Due to a lack of human data, AES wools did not receive a classification by IARC in the 2002 monographs on the evaluation of carcinogenic risks to humans (IARC, 2002). The working group also found that there was inadequate evidence in experimental animals to infer carcinogenicity. Where animal studies have been conducted, AES wools have shown little cause for concern, which is likely to be attributed to their low biopersistence *in vivo* (Bernstein et al., 1996). The reduced biopersistence of AES is due to the incorporation of soluble alkaline earth oxides, such as calcium and magnesium, into the vitreous silicate structure (Brown and Harrison, 2012; IARC, 2002), decreasing the

CONTACT Matthew S. P. Boyles  matthew.boyles@iom-world.org  Nano Safety Research Group, School of Engineering and Physical Sciences, Institute of Biological Chemistry, Biophysics and Bioengineering, Heriot-Watt University, Edinburgh, UK

 Supplemental data for this article can be accessed [here](#).

© 2018 The Author(s). Informa UK Limited, trading as Taylor & Francis Group

This is an Open Access article distributed under the terms of the Creative Commons Attribution-NonCommercial-NoDerivatives License (<http://creativecommons.org/licenses/by-nc-nd/4.0/>), which permits non-commercial re-use, distribution, and reproduction in any medium, provided the original work is properly cited, and is not altered, transformed, or built upon in any way.

half-life retention of fibers in the lung (Bellmann et al., 2010). Nose-only subchronic inhalation studies in rodents, demonstrated that long ($>20\ \mu\text{m}$) AES fibers (150 fibers/ml, 6 h/day, 5 days/week for 90 days) induced no inflammation and had considerably lower retention times than RCF. Furthermore, in existing studies, the pulmonary inflammatory response to each fiber type was found to correlate with fiber retention time (Bellmann et al., 2002; Brown et al., 2002), suggesting that fiber biopersistence influences their toxicity. In a long-term nose-only rodent inhalation study (6h/day, 5 days/week, for up to 2 years), enhanced dissolution and/or clearance of AES was shown to occur in the absence of any noteworthy biological activity. Corresponding *in vitro* tests demonstrated that dissolution of AES occurred through component leaching and transverse fragmentation (Hesterberg et al., 1998). This observation was confirmed more recently by Campopiano et al., (2014) who demonstrated rapid dissolution of AES fibers at neutral pH, concomitant with high leaching of calcium. Similarly, Osmond-McLeod et al., (2011), found considerable dissolution of AES in Gamble's solution adjusted to pH 4.5. Bernstein et al., (1996) have identified that dissolution rates at neutral pH correlated with enhanced clearance *in vivo*. Moreover, in Europe, the demonstrated low biopersistence of AES has been used to justify exoneration of AES fibers from classification under Nota-Q of the Classification, Labelling and Packaging (CLP) regulation.

As crystalline silica can be formed within HTIW during their use in high-temperature applications, concerns have recently emerged that the formation of crystalline may influence the toxicity of after-service HTIW. Upon production, RCF (consisting of alumina (Al_2O_3) and silica (SiO_2) in equal measures) and AES (consisting of varying weight ratios of silica and oxides of calcium and magnesium) have an amorphous composition (Brown and Harrison 2014). However, long-term exposure of these materials to temperatures above 1000°C is known to induce their devitrification. The dominant crystalline phases that form include cristobalite, mullite, diopside, or enstatite, although this is dependent on fiber formulation.

All of the HTIW wools tested in the present study contain excess silica which may crystallize following heating, forming cristobalite (Brown and Harrison, 2014). Crystalline silica has been classified as a Group 1 carcinogen, due to "sufficient evidence found in humans for the carcinogenicity of crystalline silica in the form of either quartz or cristobalite" (IARC, 2012). Accordingly, its formation in heated HTIW is of toxicological concern. The pathogenicity of crystalline silica is discussed in numerous review articles, and within the IARC monographs (Borm et al., 2011; Dutta and Moudgil, 2007; Guha et al., 2011; IARC, 2012; Maciejewska, 2014; Mossman and Glenn, 2013). These reviews highlight the strong epidemiological evidence, as well as *in vivo* and *in vitro* investigations which have led to the classification of crystalline silica as a carcinogen. They also provide an overview of the mechanism of crystalline silica toxicity. Much of the deleterious activity of crystalline silica stems from the reactive silanol surface groups, which bind and disrupt macromolecules, as well as generate free

radicals, which stimulates cytotoxicity, heightened immune responses, and genotoxicity lead to cancers, fibrosis (silicosis) and other serious lung disorders.

There has been relatively little research investigating the toxicity of after-service (heated) HTIW, with heated RCF receiving the most attention, to date. In a rodent nose-only inhalation study using $30\ \text{mg/m}^3$ ($220\ \text{fibers/cm}^3$, 6 h/day, 5 days/week, for 2 years), heated RCF induced respiratory lesions at a lower frequency than the unheated counterpart (Mast et al., 1995). However, "silicotic-like nodules" were observed only in rats exposed to the heated RCF (Mast et al., 1995), suggesting the development of a crystalline silica-induced pathology.

In general, existing *in vitro* studies suggest that crystalline silica-containing RCF are not more toxic than unheated RCF (Harrison and Brown, 2011). For example, in an *in vitro* study A549 (lung alveolar epithelial) cell detachment was considerably lower for after-service RCF than that observed for unheated RCF (Cullen et al., 1997). Furthermore, compared to unheated RCF, heated RCF have been shown to have a lesser effect on hamster ovarian cell proliferation and genotoxicity (Hart et al., 1992), Syrian hamster embryo (SHE) cell cytotoxicity, (Tomatis et al., 2002), red blood cell (RBC) hemolysis, and reactive oxygen species (ROS) production in granulocytes (Luoto et al., 1997). However, lactate dehydrogenase (LDH) release from macrophages exposed to unheated RCF *in vitro* was approximately half of that induced by the heated RCF, suggesting that after-service samples were more toxic (Luoto et al., 1997).

Very little is known about the biological properties of crystalline silica-containing AES fibers, and this has raised concern surrounding the perceived hazard when handling after-service HTIW. In addition it has been suggested that AES carcinogenicity classification should consider the formation of crystalline silica in the after-service product (Comodi et al., 2010). However, this is a contentious matter and the justification for this suggestion has been questioned elsewhere (Harrison and Brown, 2011). In the absence of a full assessment of the potential toxicity of cristobalite formed in fibers during use, the HTIW industry takes a precautionary stance and recommends the use of respiratory protection when handling end of life insulation materials (ECFIA, 2014).

As far as we are aware, only one study has been performed which has investigated the biological effects of after-service AES fibers (Ziemann et al., 2014). In this study, the cytotoxicity and genotoxicity induced by AES fibers in primary rat alveolar macrophages was low, and there was no evidence that responses were associated with crystalline silica.

Given the limited data on the biological response to cristobalite-containing (after-service) AES wool, and the potential hazard to workers who handle after-service AES fibers, the present study aimed to investigate the potential for heated AES fibers to induce cell death, pro-inflammatory cytokine production and ROS production *in vitro* using macrophage and alveolar epithelial cell lines. The cell models used in this study represent those found in the gas

Table 1. Physicochemical characteristics of the HTIW, including surface area, solubility, crystalline silica content, and number-weighted arithmetic mean fiber length and diameter, as well as aspect ratio and % fibers with a diameter less than 3 μm . $d_{\mu\text{m}}$ refers to the hydrodynamic diameter, and Pdl to the polydispersity index.

Material	Surface area (m ² /g)	Solubility (ppm)		Heating schedule (temp/time)	Crystalline silica content (w/w%)	Av. Length (μm)	Av. Diameter (μm)	Aspect ratio	fiber diameter <3 μm (%)
		pH 4.5	pH 7.4						
CMS-f	1.06	225.84	171.30	–	–	17.4	2.9	6.0:1	59.9
CMS-f/h	0.54	152.00	128.00	1150 °C/48h	19.4	20.0	3.9	5.1:1	37.7
MS-f	1.58	139.61	106.02	–	–	15.4	2.8	5.5:1	58.2
MS-f/h	0.58	6.32	3.51	1100 °C/60h	33.1	18.3	3.1	5.9:1	51.4
CaS-f	0.73	139.78	119.50	–	–	24.2	3.7	6.5:1	38.9
CaS-f/h	0.48	38.31	105.60	1100 °C/24h	29.4	27.1	4.7	5.8:1	24.8
RCF-f	0.64	16.19	7.49	–	–	21.3	3.8	5.6:1	42.5
RCF-f/h	0.64	5.59	5.17	1225 °C/54h	21.7	22.4	4.1	5.5:1	36.0
						$d_{\mu\text{m}}$	Pdl		
CMS-g	2.56	239.04	186.57	–	–	1.5 \pm 0.2	0.18		
CMS-g/h	0.68	125.67	60.21	1150 °C/48h	19.4 (assumed)	1.5 \pm 0.5	0.73		

Further details of the solubility assay can be seen in Table S2.

exchange region of the lungs and include macrophage (J774A.1) and alveolar epithelial (A549) cell lines. There is evidence that inhaled particles and fibers deposit in the alveolar region of the lung following pulmonary exposure (Brody et al., 1982; Oberdörster, 2002; Porter et al., 2001; van Ravenzwaay et al., 2009). Following deposition in alveoli, particles and fibers are likely to interact with alveolar epithelial cells and macrophages, promoting an inflammatory response which is key to their pathogenicity. Thus, assessment of the response of epithelial cells and macrophages is prudent when investigating the pulmonary toxicity of HTIW. The human alveolar adenocarcinoma (A549) cell line represents a type II alveolar epithelial cell (Lieber et al., 1976), and is a well-established model used in the assessment of the pulmonary toxicity of particles, including silica (Cakmak et al., 2004; Fanizza et al., 2007; Hetland et al., 2001; Monteiller et al., 2007; Schlinkert et al., 2015). Indeed, exposure of epithelial cells to fibers or silica particles *in vitro* can promote inflammatory and oxidative responses (Cakmak et al., 2004; Fanizza et al., 2007; Hetland et al., 2001; Monteiller et al., 2007). Alveolar macrophages are responsible for the clearance of inhaled particles (e.g. silica) and fibers from the lung (Geiser et al., 2008; Porter et al., 2001). Mouse macrophage J774A.1 cells are adherent, which allows a representation of the phenotypical behavior similar to that of primary alveolar macrophages (Tomlinson et al., 2012). Again this cell line is frequently used in studies which investigate the pulmonary toxicology of particles and fibers (Boyles et al., 2015; Kreyling, 1992; Marques et al., 2011), which facilitates making comparisons between the findings from the present study and existing research.

Pro-inflammatory mediators can play important roles in (pulmonary) disease progression. For example, chemoattractants such as IL-8 (the human equivalent of MIP-2), GRO- α and RANTES are implicated in the recruitment of neutrophils, and monocytes (Appay & Rowland-Jones, 2001; De Filippo et al., 2013; Scapini et al., 2004; Smith et al., 2005). In addition, the secretion of TNF- α from macrophages following exposure to quartz *in vitro* has been shown to instigate further pro-inflammatory responses (Driscoll, 2000; Driscoll et al., 1997), and MIP-2 has been identified as a vital contributor in neutrophil recruitment and acute

inflammatory responses (Driscoll, 2000). With this in mind, these pro-inflammatory mediators were considered important for us to assess.

HTIW start to devitrify into a range of forms, including crystalline silica at around 1000 °C. Only fibers in the “hot zone” of a furnace lining structure will experience such temperatures and therefore devitrify. In addition, the heat-facing wall of a fiber block is subject to severe sintering and therefore removal of fiber morphology. Within the interior of this fiber block devitrification will still occur, and in the absence of sintering will result in fibers containing crystalline silica being formed. Further distance from the heat source is associated with limited or no crystallization (Ganz & Krönert, 1982). Therefore, the present study has focused on the limited proportion of fibers that would be exposed to high temperature during use and that also maintain a fibrous form.

Cells were exposed to RCF and three distinct AES, of different compositions. All test materials were studied in a heated and unheated form. Additional treatments included DQ12 α -quartz as a positive crystalline silica control and TiO₂ as a particle negative control. Aluminum lactate coating was used to distinguish between crystalline silica-induced effects and those not associated with crystalline silica, as has previously been shown (Duffin et al., 2001).

Methods

Chemicals and materials

The HTIW under investigation are all in commercial production, but the manipulations were done specifically for this study by Morgan Advanced Materials (Bromborough, UK) and were provided to Heriot-Watt University in a coded form to allow *in vitro* experiments to be blinded. DQ12 quartz was donated by the Institute of Occupational Medicine (IOM) (Edinburgh, UK) (DQ12 was included in this study as a positive control for effects pertaining to crystalline silica); TiO₂ was from Tioxide, UK; nanoparticle carbon black (NPCB) was obtained from Degussa (Printex 90). rhTNF- α was from Immunotools (Friesoythe, Germany); AlamarBlue reagent, GibcoTM Penicillin-Streptomycin, RPMI 1640, phenol red-free MEM were from Thermo Fisher

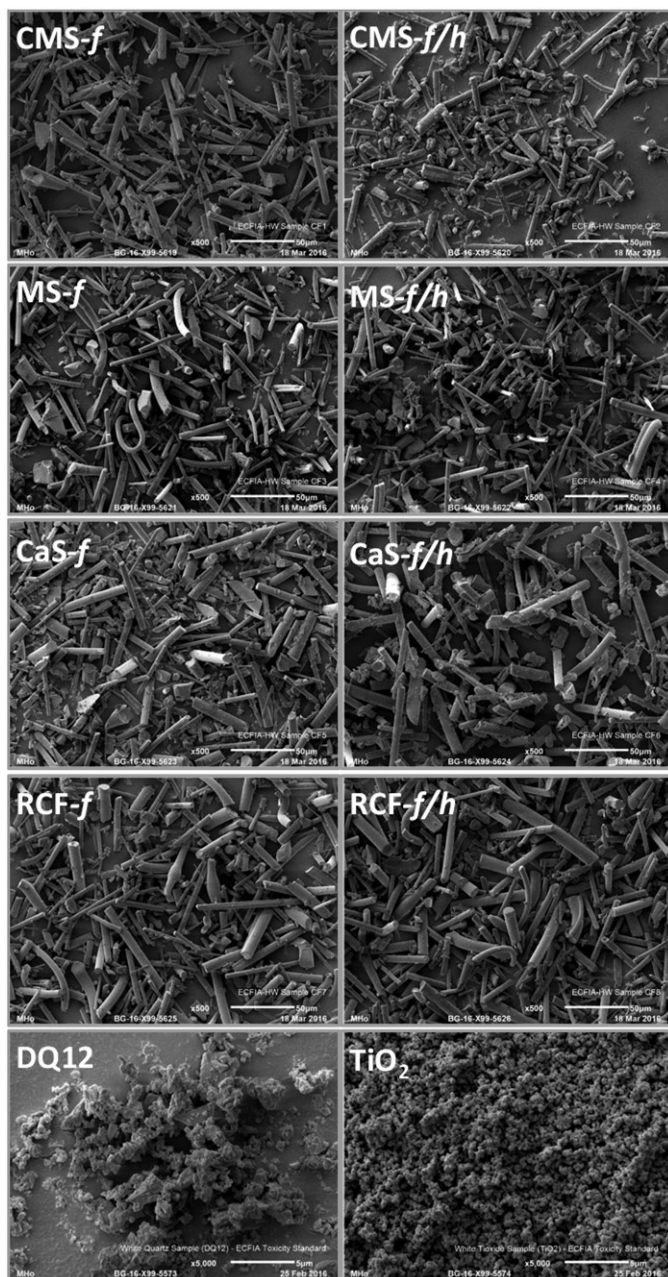


Figure 1. Scanning electron microscopy images of the fibers and particles investigated, including CMS-*f* (unheated fibers), CMS-*f/h* (heated fibers), MS-*f* (unheated fibers), MS-*f/h* (heated fibers), CaS-*f* (unheated fibers), CaS-*f/h* (heated fibers), RCF-*f* (unheated fibers), RCF-*f/h* (heated fibers). The scale of each image is included at the bottom right of each image, and represents 50 μm on the HTIW images, and 5 μm on the images of DQ12 and TiO_2 .

(Paisley, UK); QCL-1000 Endpoint Chromogenic LAL Assay was from Lonza (Slough, UK); Proteome Profiler Cytokine Array Kit, Magnetic Luminex Screening Assay, and DuoSet ELISA kits were from R&D Systems (Abingdon, UK); 1-hydroxyl-2,2,6,6-tetramethyl-4-oxo-piperidine (Tempone-H) was from Enzo Life Sciences (Exeter, UK). All other substances used were obtained from Sigma-Aldrich (Poole, UK).

Preparation and characterization of HTIW samples

The chemistry of the four HTIW were calcium magnesium silicate wool (CMS), magnesium silicate wool (MS), calcium

silicate wool (CaS) and aluminosilicate wool (ASW; also known as refractory ceramic fibers, RCF). Alongside the acronyms identified above, each material was further classified with the following suffixes: *-f* meaning fiber, *-f/h* for heated fiber, *-g* for ground, and *-g/h* for heated ground material.

The original bulk material was initially broken and passed through a 6 mm mesh, to reduce the fiber length from that of manufacture. Two stages of air processing were performed: de-shotting and coarse fiber removal, using a 50 ATP Air Classifier. This process was chosen to prepare samples that would be similar to workplace fibrous dust, with a corresponding respirable fraction. A portion of these samples were then ground in a Tema mill to produce a nonfibrous, ground sample for comparative testing.

The heated fibers (*f/h*) and heated ground (*g/h*) samples were prepared by taking a fraction of the unheated material and heating in an Elite BRF 16/21 furnace for the specified time and temperature. The treatment was different for each HTIW chemistry and the details are given in Table 1. The target was to achieve close to full crystallization for each sample while avoiding excessive sintering. The crystalline silica proportion given in Table 1 is close to the maximum feasible for each HTIW chemistry. CMS-*f/h*, *-g/h* and RCF-*f/h*, *-g/h* contained approximately 20% crystalline silica and CaS-*f/h*, *-g/h* and MS-*f/h*, *-g/h* contained approximately 30%. The fibrous samples were assessed for crystalline silica content, which was then used to estimate valEEues for the ground samples. Estimation rather than measurement was conducted due to the small mass/volume available for the ground samples, and the fact that the fibrous and ground samples were fired simultaneously therefore receiving the same heat treatment for the same period of time. This does not affect the conclusions made in the assessment of the fibrous HTIW under investigation here.

As heat treatment sinters the particles together, sonication (at 0 °C in dH_2O for 2 h using a sonicating water bath (James Products Europe Sonic 6MX)) was used to separate individual fibers. The low temperature was utilized to minimize leaching of ions from the test materials. Remaining agglomerates were removed with a Plastok 30 μm Nylon sieve. The pristine samples (unheated fibers) also underwent the same process to keep all sample preparation uniform. The sieved materials were dried in Pyrex dishes overnight at 120 °C, and then heated at 650 °C to remove any adsorbed moisture or organics (including bacterial endotoxin).

Sample chemistry was determined using a PANalytical X-Ray Fluorescence analyzer after each stage of preparation to check there was no potential contamination and that the chemistry remained near-identical to the starting fiber. All samples were imaged using a JEOL SEM to confirm particles remained separate and no irregularities were introduced. Number weighted fiber size distributions were generated using a Malvern Morphology G2 particle size analyzer, with the mean diameter and lengths of at least 2000 samples reported.

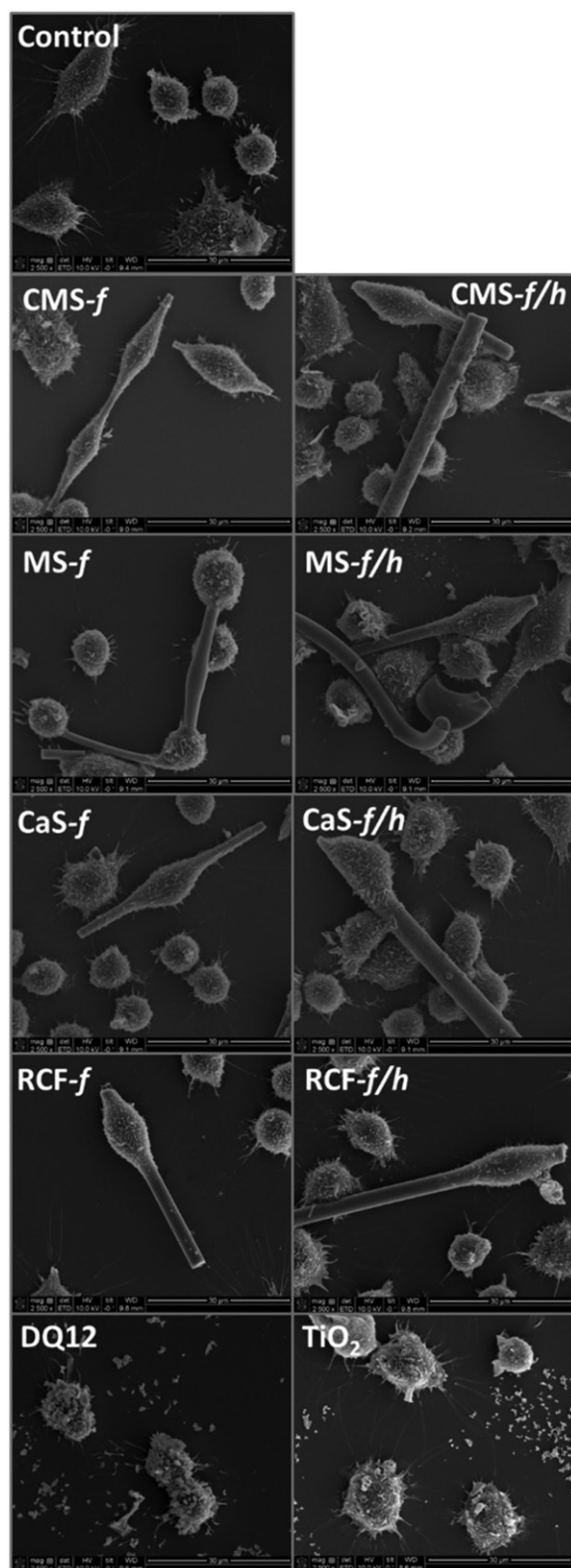


Figure 2. SEM images of untreated/control J774A.1 cells, and cell treated with CMS-*f* (unheated fibers), CMS-*f/h* (heated fibers), MS-*f* (unheated fibers), MS-*f/h* (heated fibers), CaS-*f* (unheated fibers), CaS-*f/h* (heated fibers), RCF-*f* (unheated fibers), RCF-*f/h* (heated fibers). Cells were exposed to $40 \mu\text{g}/\text{cm}^2$ for 24 h prior to SEM preparation, and imaged using a FEI Quanta 3D FEG scanning electron microscope. A scale bar is shown at the bottom right corner of each image.

Determination of endotoxin contamination

All test materials and control particles were suspended in endotoxin-free water or water spiked with endotoxin at $0.5 \text{ EU}/\text{mL}$. These suspensions were incubated for 24 h under cell culture conditions. Each suspension media served as the negative vehicle control. After the incubation period, each sample was centrifuged at $21,000 \times g$ for 10 min to remove test materials, and the level of endotoxin was quantified using a Limulus Amebocyte Lysate (LAL)-based detection method, following manufacturer's instructions.

Characterization of DQ12 and TiO₂

Hydrodynamic size distributions and relative sample dispersity (polydispersity index (PDI)) of DQ12 and TiO₂ were assessed at $100 \mu\text{g}/\text{mL}$ by dynamic light scattering (DLS) using a Malvern ZetaSizer Nano ZS (Malvern Instruments, Malvern, UK) operating with a light source wavelength of 532 nm and a fixed scattering angle of 173° . DQ12 was determined to be 100% Quartz by XRD, with a hydrodynamic diameter of $802 (\pm 38) \text{ d.nm}$ in water and $643 (\pm 139) \text{ d.nm}$ in cell culture medium, with PDI of 0.41 (± 0.05) and 0.88 (± 0.18), respectively. TiO₂ was determined to be 95.4% rutile and 4.2% anatase, by XRD, with a hydrodynamic diameter of $472 (\pm 7) \text{ d.nm}$ in water and $754 (\pm 2) \text{ d.nm}$ in cell culture medium, with PDI of 0.13 (± 0.04) and 0.20 (± 0.04) respectively.

Solubility assessment of HTIW

Static solubility testing was conducted, in duplicate, on all samples for 24 h. Each sample was suspended at $20 \text{ mg}/\text{mL}$ in simulated body fluids. These included optimized Gamble's solution at pH 7.4, and optimized artificial lysosomal fluid (ALF) at pH 4.5. Gamble's solution refers to an extracellular fluid, first described by J. L. Gamble in 1967 (Gamble, 1967) and has been routinely used to model the durability of materials such as glass fiber in extracellular fluid (Kokubo et al., 1987), including when fibers are deposited within the lungs (Alexander et al., 1994). The Gamble's formulation used here consisted of sodium chloride (NaCl) $6.780 \text{ g}/\text{L}$, sodium hydrogen carbonate (NaHCO_3) $2.268 \text{ g}/\text{L}$, ammonium chloride (NH_4Cl) $0.535 \text{ g}/\text{L}$, sodium citrate dihydrate ($\text{Na}_3\text{C}_6\text{H}_5\text{O}_7 \cdot 2\text{H}_2\text{O}$) $0.059 \text{ g}/\text{L}$, glycine ($\text{NH}_2\text{CH}_2\text{CO}_2\text{H}$) $0.450 \text{ g}/\text{L}$, di-sodium hydrogen orthophosphate anhydrous (Na_2HPO_4) $0.171 \text{ g}/\text{L}$, formaldehyde 2.5 mL , and sulfuric acid (1:10 dilution in dH_2O) $0.490 \text{ g}/\text{L}$. For ALF, the following components were used: sodium chloride (NaCl) $7.120 \text{ g}/\text{L}$, sodium hydrogen carbonate (NaHCO_3) $1.950 \text{ g}/\text{L}$, di-sodium orthophosphate (Na_2HPO_4) $0.148 \text{ g}/\text{L}$, sodium sulfate (Na_2SO_4) $0.079 \text{ g}/\text{L}$, glycine ($\text{NH}_2\text{CH}_2\text{CO}_2\text{H}$) $0.118 \text{ g}/\text{L}$, tri-sodium citrate ($\text{Na}_3\text{Citrate} \cdot 2\text{H}_2\text{O}$) $0.152 \text{ g}/\text{L}$, sodium L-tartrate dihydrate ($\text{Na}_2\text{tartrate} \cdot 2\text{H}_2\text{O}$) $0.180 \text{ g}/\text{L}$, sodium pyruvate (Na-pyruvate) $0.172 \text{ g}/\text{L}$, 90% lactic acid $0.156 \text{ g}/\text{L}$, formaldehyde $1.5 \text{ mL}/\text{L}$, with pH adjustment to 4.5 using HCl. Samples were agitated in a Memmert WB22 water bath for 24 h at 37°C . Upon removal, the samples were

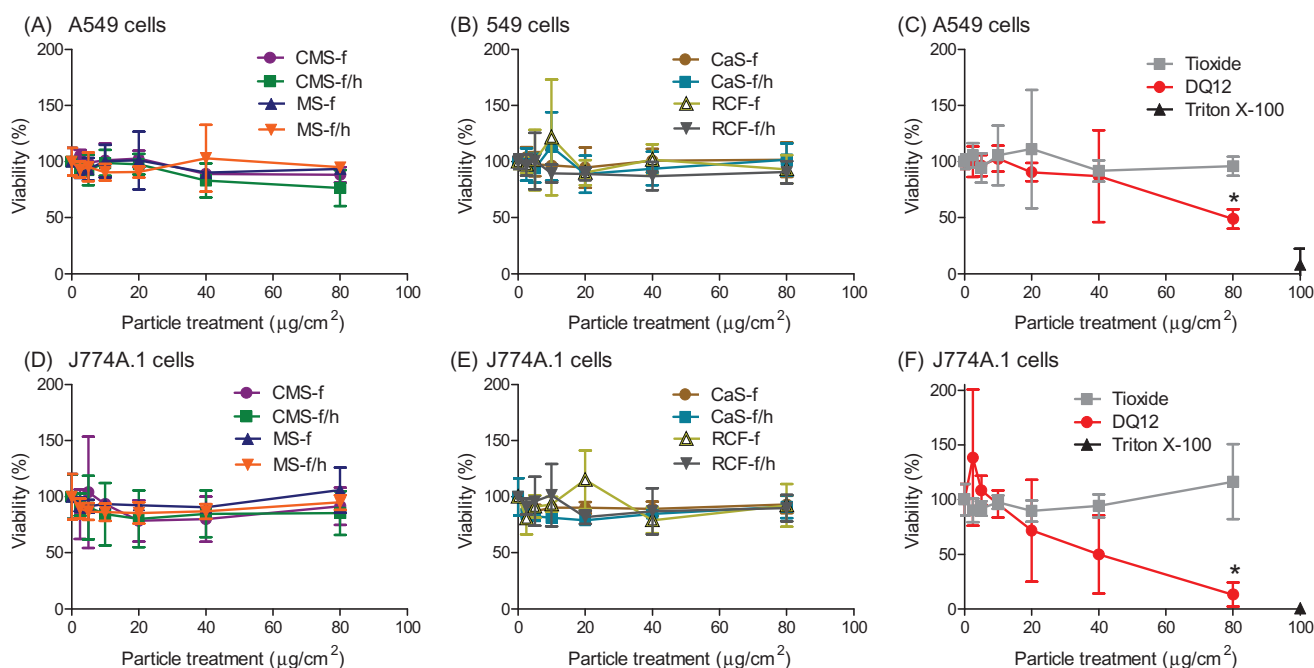


Figure 3. Cell viability, determined by mitochondrial activity (AlamarBlue assay), in response to HTIW. A-C) A549 cells and D-F) J774A.1 cells were treated for 24 h with 0–80 $\mu\text{g}/\text{cm}^2$ heated and unheated CMS-f, MS-f, CaS-f and RCF-f, as well as particle controls DQ12 and TiO_2 . Results are expressed as % viability compared to vehicle (medium-only) control, and each data point represents the mean \pm SD of at least three independent biological replicates. Statistical significance of particle exposures in comparison to medium only is indicated with * when $p < 0.05$.

filtered using Whatman Ashless 21:45- μm filter paper and analyzed using a SpectroFlame Modula ICP-OES system.

Cell culture and treatment

The immortalized A549 human lung alveolar adenocarcinoma and J774A.1 mouse macrophage-like cell lines, were maintained at 37°C with 5% CO_2 under sterile conditions. The growth medium consisted of RPMI 1640 supplemented with 10% heat-inactivated FCS, 1% L-glutamine, 100 U/mL penicillin, and 100 $\mu\text{g}/\text{mL}$ streptomycin. Cells were seeded one day prior to experiments in 96-well plates (100 μl /well) unless stated otherwise. A549 cells were seeded at a density of 2×10^5 and J774A.1 cells at 1.6×10^5 cells per cm^2 . Cells were exposed to HTIW (fibrous and ground), DQ12, or TiO_2 at concentrations of 0–80 $\mu\text{g}/\text{cm}^2$ (dependent on endpoint), for 4–24 h (dependent on endpoint). All of the ground counterparts were tested alongside the fibrous material, as were the positive and negative particle control treatments. This had the benefit of allowing fiber effects to be separated from effects dependent on other material characteristics. The data obtained by ground sample exposures provided useful comparative information, but are presented within this manuscript only when specific comparisons were necessary. In all assays, a vehicle control acted as negative control. The positive controls varied depending upon the assay and cell type, and included Triton X-100 for cytotoxicity and viability assays, rhTNF- α (20 ng/mL) for A549-induced pro-inflammatory mediator release, lipopolysaccharide (LPS) (100 ng/mL) for J774A.1-induced pro-inflammatory mediator release, as well as nanoparticle carbon black (NPCB) (2.5–20 $\mu\text{g}/\text{cm}^2$) and *tert*-Butyl hydroperoxide (tBHP) (0.1–10 mM) for ROS generation.

Uptake assessed by scanning electron microscopy

J774A.1 cells were cultivated in 24 well plates on sterile cover slips and treated with 40 $\mu\text{g}/\text{cm}^2$ of all test material for 24 h, as described above. The exposure medium was then removed and cells washed with PBS. The samples were then fixed for 180 min in a solution containing 2.5% glutaraldehyde in 0.1 M sodium cacodylate buffer. After this period, cells were washed three times with 0.1 M sodium cacodylate buffer prior to dehydration through the addition of increasing concentrations of EtOH (in dH_2O) until the samples were in 100% EtOH. The samples were then dried using hexamethyldisilazane, mounted onto SEM stubs and sputter coated with gold prior to examination using a FEI Quanta 3 D FEG microscope.

Cytotoxicity and cell viability

Cytotoxicity – lactate dehydrogenase (LDH) quantification

To assess LDH released from cells (indicative of cell membrane impairment) 24-h postexposure. A549 and J774A.1 cells were exposed to the test materials for 24 h at a range of concentrations, and LDH activity was assessed in supernatants via assessment of pyruvate concentration. The assay used works on the principle that the concentration of pyruvate is inversely proportional to the concentration of LDH, as previously described (Boyles et al., 2015; Brown et al., 2001).

Viability – AlamarBlue and neutral red uptake (NRU)

The assessment of viability using the AlamarBlue and neutral red assays was performed using an adaption of the protocol described by Connolly et al., (2015); both of these

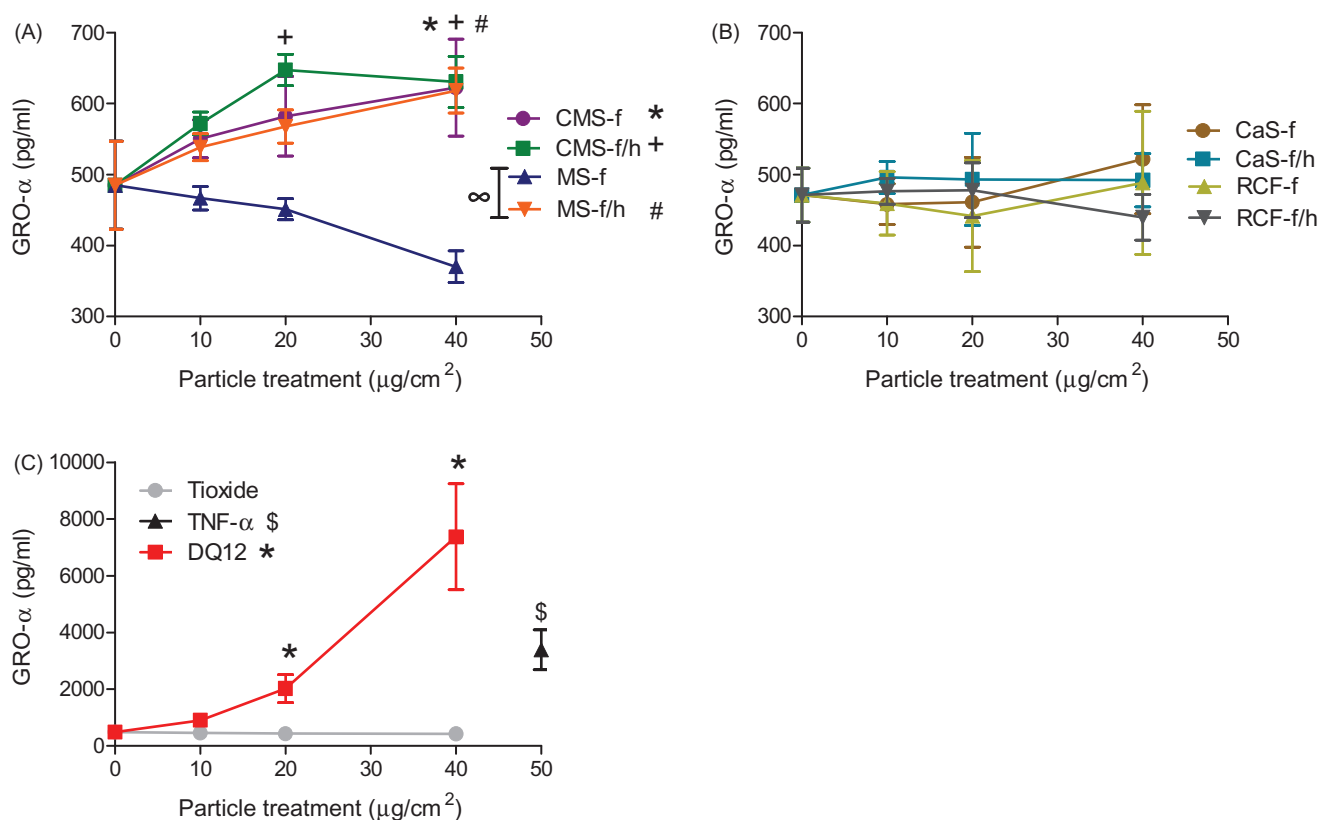


Figure 4. GRO- α release from A549 cells treated for 24 h with 0–40 $\mu\text{g}/\text{cm}^2$ heated and unheated CMS-*f*, MS-*f*, CaS-*f* and RCF-*f*, as well as particle controls DQ12 and TiO₂. Each data point represents the mean \pm SD of at least three independent biological replicates. Statistical significance of particle exposures in comparison to medium only is indicated when $p < 0.05$, identifying markers are shown on corresponding legends, and with ∞ when a heated sample is significantly different to an unheated sample.

tests were conducted on the same cell populations. After 24 h of exposure, the medium was removed and cells washed twice with PBS. A solution of phenol red-free MEM containing 1.25% (v/v) AlamarBlue reagent was then added to cells and incubated in normal cell culture conditions for 1 h, protected from light. After this time period, the plate was read for fluorescence intensity at ex/em wavelengths of 532/590 nm, on a SpectraMax M5 plate reader. The cells were then washed once with PBS prior to addition of 33 $\mu\text{g}/\text{mL}$ neutral red solution for 1 h. The cells were then washed twice before addition of lysis buffer (1% acetic acid, 50% EtOH, and 49% dH₂O). Any neutral red dye released, representing the fraction previously held within lysosomes, was quantified by measuring fluorescence intensity at ex/em wavelengths of 532/645 nm.

Assessment of pro-inflammatory mediators – multiplex analysis

Prior to performing the multiplex analysis of secreted proteins, a pre-selection process was performed to ensure that relevant inflammatory mediators were assessed. Cells were exposed to DQ12, CMS-*f* and CMS-*f/h* for 24 h, and a protein array of 36 cytokines, chemokines, or acute phase proteins for A549 cells, and 40 cytokines, chemokines, or acute phase proteins for J774A.1 cells were used to assess cytokine production in the cell supernatants (data not shown). Based on which mediators were found to be induced by either DQ12 or CMS, or to both, the following

proteins were selected for further investigation using multiplex analysis: A549 cell supernatant was assessed for MCP-1, GRO- α , IL-6, IL-8, and RANTES, and J774A.1 cell supernatant for G-CSF, IL-1 β , RANTES, TNF- α , GM-CSF, and MIP-2.

The release of pro-inflammatory biomarkers from A549 and J774A.1 cells was assessed using a multiplex system, Magnetic Luminex Screening Assay, for mouse or human analytes. Due to the substantial cell death observed during 24 h in response to the highest concentration of DQ12 (80 $\mu\text{g}/\text{cm}^2$), exposures of 0–40 $\mu\text{g}/\text{cm}^2$ were used for the study of pro-inflammatory responses. The analysis was performed following the manufacturer's guidelines.

Measurement of acellular reactive oxygen species generation

Acellular ROS determination: DCFH oxidation

The method used to determine acellular DCFH oxidation included an initial step for chemical hydrolysis of DCFH-DA to DCFH in an NaOH solution prior to addition of DCFH to particle suspensions; this process is described in more detail elsewhere (Rothen-Rutishauser et al., 2010). Background measurements of signals obtained at time zero were subtracted from each time point, and vehicle only fluorescence values were subtracted from test material values. Autofluorescence was assessed by performing

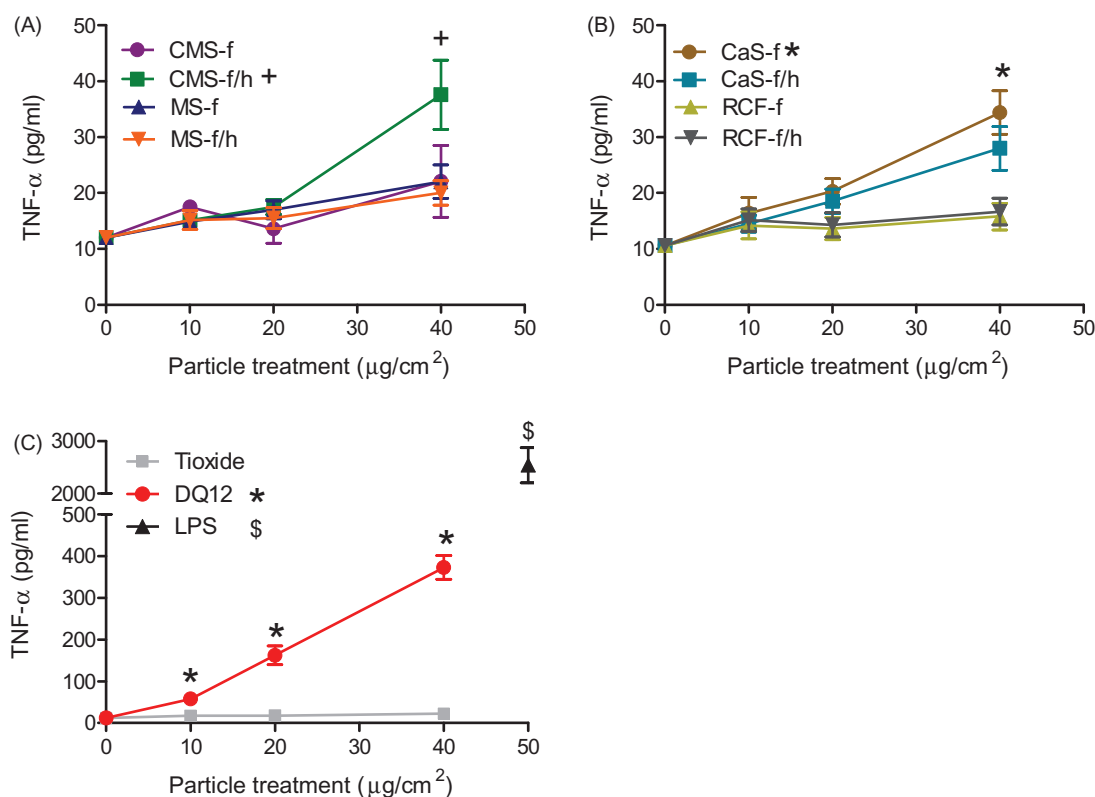


Figure 5. TNF- α release from J774A.1 cells treated for 24 h with 0-40 $\mu\text{g}/\text{cm}^2$ heated and unheated CMS-f, MS-f, CaS-f and RCF-f, as well as particle controls DQ12 and TiO₂. Each data point represents the mean \pm SD of at least three independent biological replicates. Statistical significance of particle exposures in comparison to medium only is indicated when $p < 0.05$, identifying markers are shown on corresponding legends.

this assay in the absence of DCFH-DA; none was found (data not shown).

Acellular ROS determination: superoxide generation

Due to differences in the specificity of ROS detected, electron paramagnetic resonance (EPR) was also used to establish ROS generated by the test materials in the absence of cells. The spin trap 1-hydroxyl-2,2,6,6-tetramethyl-4-oxo-piperidine (Tempone-H) was made up in 0.01 M EDTA at 100 mM (final concentration of 1 mM) and stored on ice until used. All particles were suspended at 1 mg/mL in Milli-Q water and sonicated for 10 min, with final dilutions giving 125 $\mu\text{g}/\text{mL}$ for were DQ12, TiO₂ and HTIW, and 16 and 32 $\mu\text{g}/\text{mL}$ for NPCB; these concentrations directly correspond to those used in the assays involving culture plates. Pyrogallol (a positive control superoxide radical generation (Miller et al., 2009)) was prepared in a Krebs buffer to give a final concentration of 32 μM . All samples were maintained at 37 $^{\circ}\text{C}$, and measurements were taken 60 min after addition of Tempone-H. Up to 50 μL of sample were drawn into capillary tubes and sealed using a soft sealant. Using a Miniscope MS 200 (Magnettech, Berlin, Germany), the EPR spectrum was obtained with the following parameters: microwave frequency, 9.3–9.55 Hz; microwave power, 20 mW; modulation frequency, 100 kHz; modulation amplitude, 1,500 mG; center field, 3,350 G; sweep width, 55 G; sweep time, 30 sec; number of passes, 1.

Cellular reactive oxygen species generation

We have previously determined that when a slow but consistent formation of intracellular ROS is generated in response to particle treatments, it is more suitable to apply an extended particle treatment before loading cells with DCFH-DA (Pang et al., 2017). Therefore, prior to intracellular detection of ROS, each cell line was treated as previously described to HTIW, DQ12, or TiO₂, at 0-40 $\mu\text{g}/\text{cm}^2$, for 4 or 12 h. An additional control included NPCB (0–20 $\mu\text{g}/\text{cm}^2$), which provides high levels of ROS generation (Foucaud et al., 2007; Rothen-Rutishauser et al., 2010). After treatment, the medium was removed and the cells were washed once with HBSS (w. Mg and Ca) before addition of 25 μM DCFH-DA in HBSS and incubation at 37 $^{\circ}\text{C}$. Cleavage of DCFH-DA to DCFH by intracellular esterases, allowed detection of intracellular DCFH oxidation, measured on a SpectraMax M5 plate reader 6 h after addition of DCFH-DA, using ex/em wavelengths of 485 nm/530 nm. Vehicle only fluorescence values were subtracted from test material values. Autofluorescence was assessed by performing this assay in the absence of DCFH-DA, none was found.

Aluminum lactate coating and assessment of its biological impact on HTIW effects

Material coating and cell treatment

Only those materials which had previously induced a statistically significant release of pro-inflammatory mediators in the multiplex analysis were used for these further tests. Coating

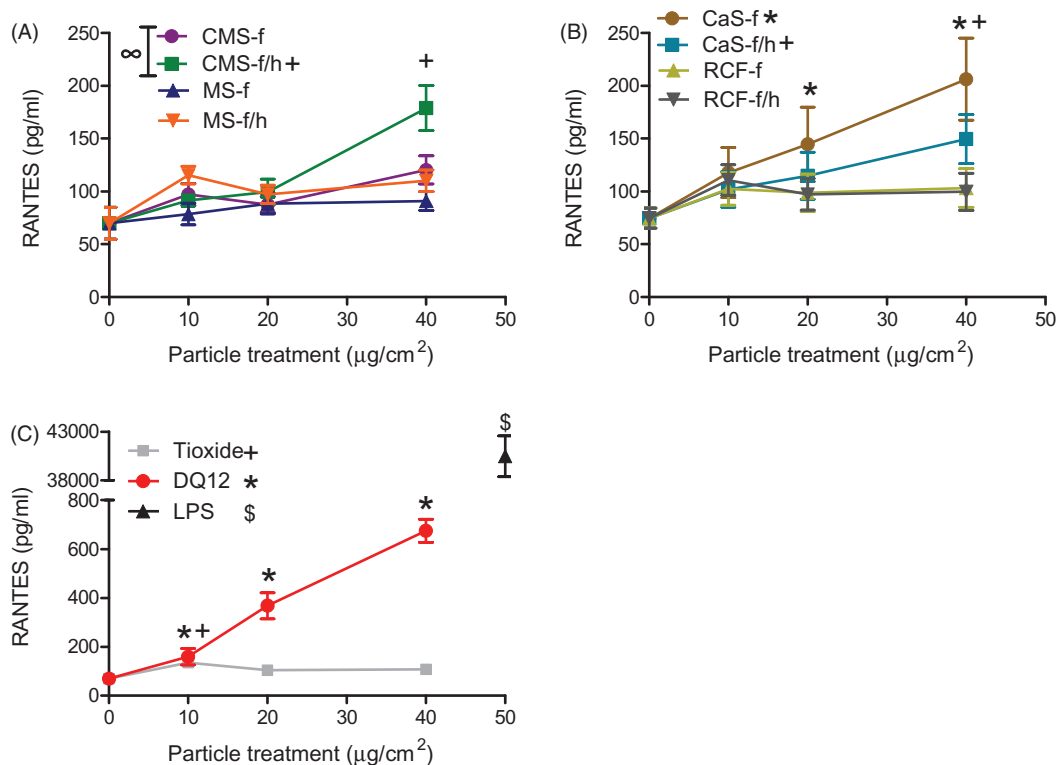


Figure 6. RANTES release from J774A.1 cells treated for 24 h with 0–40 µg/cm² heated and unheated CMS-*f*, MS-*f*, CaS-*f* and RCF-*f*, as well as particle controls DQ12 and TiO₂. Each data point represents the mean ± SD of at least three independent biological replicates. Statistical significance of particle exposures in comparison to medium only is indicated when $p < 0.05$, identifying markers are shown on corresponding legends, and with ∞ when a heated sample is significantly different to an unheated sample.

of materials with aluminum L-lactate (AL) was performed as previously described by Duffin *et al.*, (2001). Briefly, 100 mg AL was dissolved in 10 ml phosphate-buffered saline (PBS). Test materials were suspended at 5 mg/mL in AL, with control particles suspended at 5 mg/mL in PBS. Each sample was briefly vortexed prior to sonication in a sonicating bath (Ultrawave, Q-Series Ultrasonic Bath, 400W) for 10 minutes. After which, both suspensions were rotated in a rotating sample mixer for at least 3 h at room temperature. The samples were then transferred to Eppendorf tubes (in 1 ml aliquots) and washed: Eppendorf tubes were centrifuged at 21000×*g* for 10 min, 1 ml of the supernatant was removed without disturbing the pellet, then the pellet was resuspended in 1 ml PBS. This wash step was performed twice, and samples were finally resuspended and diluted in cell culture medium to provide treatments at 0–40 µg/cm². Suspensions were added to cells for 24 h, after which supernatant was removed for the analysis of secreted protein by ELISA.

Enzyme-linked immunosorbent assay (ELISA)

Secretion of pro-inflammatory cytokines GRO-α (A549 cells), TNF-α, RANTES, and MIP-2 (J774A.1 cells) in response to test materials were assessed in cell supernatants by ELISA following the manufacturer's instructions.

Overall study design

The different responses measured in this study are unlikely to occur simultaneously, instead they can occur in a

sequence that is related to the mechanism of bioreactivity. One such example involves ROS and oxidative stress, in which the secretion of pro-inflammatory mediators occurs as a consequence of ROS generation, and cell death occurs subsequent to ROS production and cytokine release (Nel *et al.*, 2006). Therefore, we assessed ROS production as early as 1 h, and continued up to 24 h post-exposure. The positive control treatments of NPCB and tBHP were shown to cause ROS production within the first time points assessed (data not shown), while responses to the other materials developed slowly over time, with optimal time points identified to be 4 and 12 h. The timing of release of different pro-inflammatory cytokines may also vary, especially when cells are responding to different stimuli. For example the release of TNF-α from J774A.1 cells has been shown to occur much earlier than MIP-2 in response to polyamidoamine dendrimers (Naha *et al.*, 2010), while LPS has been shown to induce the simultaneous and early (within 2 h) release of both TNF-α and MIP-2. Here, we found substantial release of both these proteins at 4-h postexposure (data not shown), as well as 24 h, in response to our positive control treatments of LPS and DQ12. We have relied upon detection of these mediators within the supernatant after a 24 h exposure period has elapsed. Using recombinant proteins, the concentration of TNF-α and IL-1β have both been shown to reduce when stored at 37 °C, for example TNF-α concentration dropped by approximately 40% and IL-1β by 20%, an effect not shown when proteins were stored at 4 °C (Piret *et al.*, 2017). Although this may have an impact on the proteins remaining intact and available for detection here, it

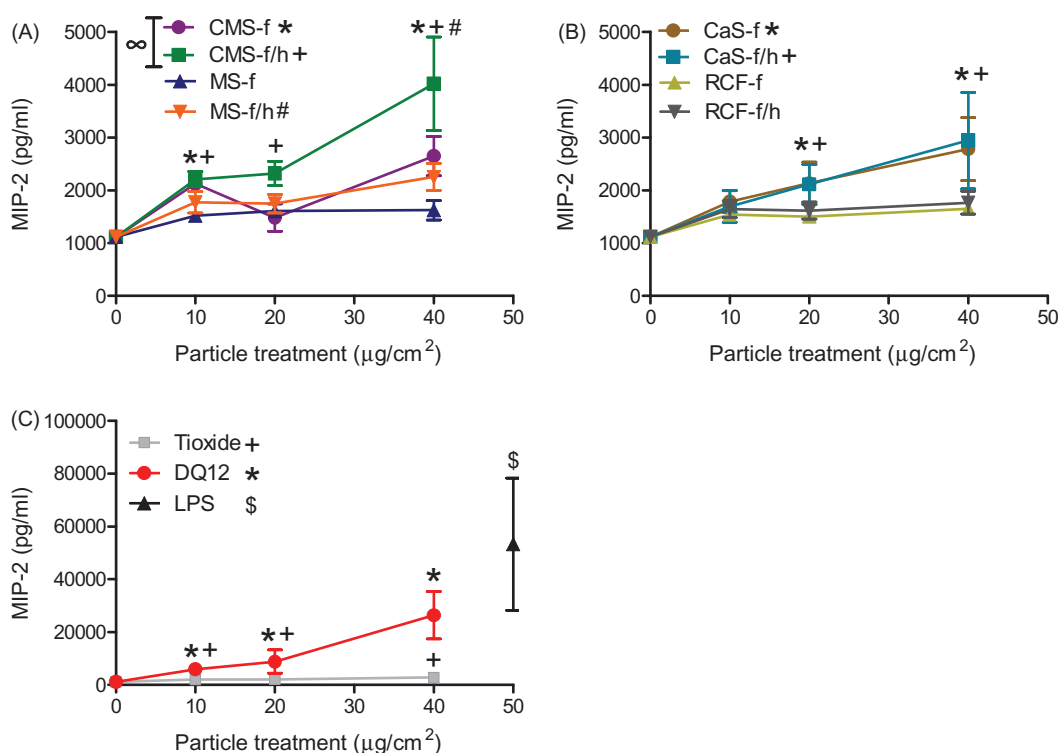


Figure 7. MIP-2 release from J774A.1 cells treated for 24 h with 0-40 $\mu\text{g}/\text{cm}^2$ heated and unheated CMS-*f*, MS-*f*, CaS-*f* and RCF-*f*, as well as particle controls DQ12 and TiO_2 . Each data point represents the mean \pm SD of at least three independent biological replicates. Statistical significance of particle exposures in comparison to medium only is indicated when $p < 0.05$, identifying markers are shown on corresponding legends, and with ∞ when a heated sample is significantly different to an unheated sample.

should be noted that we have an ongoing exposure with particle:cell interactions continuing throughout the 24 h, and moreover, the effect would be relative across exposure samples, therefore comparisons between treatments would carry the same relevant significance.

Statistical analysis

Data was analyzed with SPSS, using a general linear model for multivariate analysis with Tukey's post hoc analysis when data was deemed to have a normal distribution, and using Kruskal-Wallis 1-way ANOVA with all pairwise comparison when data not found to be normally distributed. Statistical significance is given with a 95% confidence interval, that is, when p -value ≤ 0.05 .

Results

Characterization

Four different HTIW were used; three AES wools and RCF (ASW). Using SEM, it was observed that each of the HTIW samples exhibited a fibrous morphology (Figure 1). There was no clear modification observed upon heating of these materials, and fibrous morphology was maintained (Figure 1). However, as these samples were sonicated to separate sintered material, we cannot rule out the possibility that ultra-sonication may have exposed crystalline silica at the sites where the sintering bonds were fractured. The size

of DQ12 is often reported in the literature as less than $5 \mu\text{m}$ (Ernst et al., 2002; Kolling et al., 2011; Lasfargues et al., 1992; Sawyer et al., 1981), which is reflected in the SEM images presented. TiO_2 particle size is reported in the literature to be 250 nm (Barlow et al., 2005; Renwick et al., 2004), which is also confirmed by SEM.

Each sample was chosen to be compositionally distinct; this was confirmed by compositional analysis (Table S1). Other characteristics, including fiber dimensions, surface area and percent crystalline silica content are presented in Table 1. XRD analysis of MS-*f/h*, CaS-*f/h* and RCF-*f/h* demonstrated the presence of cristobalite. Other crystalline silica polymorphs such as quartz and tridymite were not detected. Cristobalite was the main polymorph formed in CMS-*f/h*, however 0.9% tridymite was also identified.

Surface area of the test materials was measured using BET. This method quantifies gas adsorption and although accurate for specific surface area may not reflect the true bioavailable surface area (Meißner et al., 2010; Oberdörster et al., 2015). The characteristics of DQ12 and TiO_2 are given in the methods section. The hydrodynamic diameter for TiO_2 can be considered reliable, as the PDI value for these measurements is relatively low (0.20 ± 0.04) with a reasonably uniform size distribution, also observed by SEM (Figure 1). In contrast, the hydrodynamic diameter for DQ12 was not considered to be a good representative for the sample as a whole, as the PDI approached 1 (0.88 ± 0.18), reflecting the heterogeneity of DQ12 size, also observed by SEM (Figure 1).

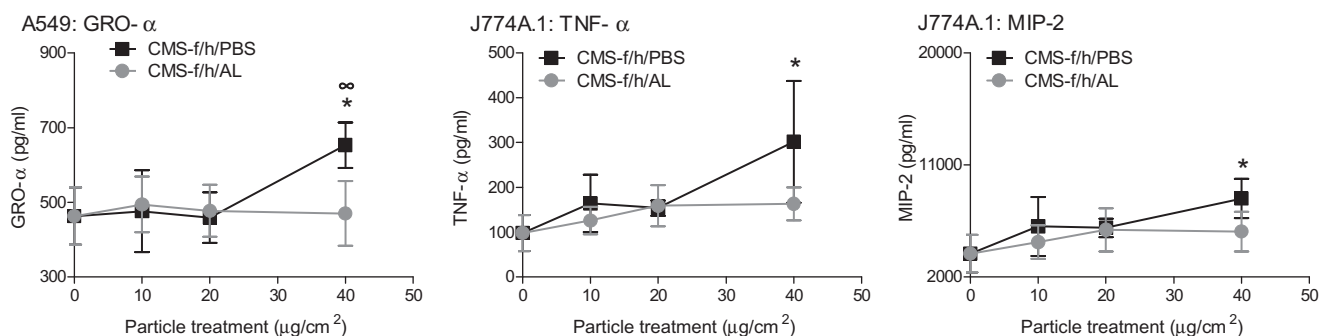


Figure 8. Effect of aluminum lactate coating on the release of pro-inflammatory mediators, including GRO- α from A549 cells (A), and TNF- α (B) and MIP-2 (C) from J774A.1 cells. Cells were treated for 24 h with 0–40 $\mu\text{g}/\text{cm}^2$ heated, crystalline silica-containing CMS-*f/h*. The test material was either coated with AL (grey lines) or processed in the same fashion in PBS without AL (black lines). Each data point represents the mean \pm SD of at least three independent biological replicates. Statistical significance of PBS processed particles compared to medium only is indicated with * when $p < 0.05$, and when AL coating is significantly different without AL with ∞ when $p < 0.05$.

Fiber uptake

The interaction of fibers with the macrophage J774A.1 cell line was assessed by SEM (Figure 2). From these images, uptake by cells of all fibers tested was clearly evident; moreover, each fiber tested was of a dimension which could induce frustrated phagocytosis. Cells were also observed to take up the positive and negative particle controls, DQ12 and TiO₂, respectively.

Cytotoxicity

To indicate what effect the treatments had upon cell death and cell viability over 24 h, mitochondrial function (Figure 3), the ability of cells to incorporate neutral red within lysosomes (Figure S1), and the release of LDH (Figure S1) were determined. None of the three AES materials nor the RCF induced cell death or reduced viability in either cell type, this was true whether the samples were heated or unheated, or in ground or fibrous forms. This was also true for the negative particle control, TiO₂. Conversely, DQ12 induced significant cell death. This was evident in all three assays and in both cell lines, although J774A.1 cells appeared more sensitive than A549 cells.

Pro-inflammatory responses

As the highest concentration of DQ12 (80 $\mu\text{g}/\text{cm}^2$) was found to be extremely cytotoxic, this concentration was no longer used to assess pro-inflammatory mediator release. Instead, each cell type was treated with 0–40 $\mu\text{g}/\text{cm}^2$ of all test materials, as this represented a sublethal concentration range at the time point (24 h) used.

A549 cell supernatant was assessed for RANTES, MCP-1, IL-6, IL-8 and GRO- α . GRO- α was significantly increased in response to MS-*f/h* and both CMS-*f* and CMS-*f/h* (Figure 4(A)). However, these responses were over 10 fold lower than the cells' response to DQ12 (Figure 4(C)). Treatments of CaS and RCF did not induce cytokine release greater than the medium only control (Figure 4(B)). The positive control TNF- α induced the release of all of the cytokines tested, while DQ12 induced significant release of all of the tested pro-inflammatory

mediators except RANTES (Figure S2). In contrast, the negative control TiO₂ induced no release of pro-inflammatory mediators in A549 cells.

J774A.1 cell supernatants were assessed for TNF- α , RANTES and MIP-2 (Figures 5–7), as well as G-CSF, IL-1 β and GM-CSF (Figure S3). Upon treatment of J774A.1 cells with the HTIW, only CMS-*f/h* and CaS-*f* induced a significant release of TNF- α (Figure 5). Similarly to the effect observed in the release of GRO- α from A549 cells, TNF- α released from J774A.1 cells in response to DQ12 was approximately 10-fold more than in response to HTIW (Figure 5(C)).

CMS-*f/h*, CaS-*f* and CaS-*f/h* fibers induced a significant release of RANTES from J774A.1 cells (Figure 6). In contrast, neither MS nor RCF caused any change in RANTES compared to the medium only control. The secretion of RANTES was 3–5-fold greater in response to DQ12 than to HTIW (Figure 6(C)). TiO₂ was also found to induce a low, but significant release of RANTES, but only at the lowest concentration of 10 $\mu\text{g}/\text{cm}^2$, this response was not maintained at higher concentrations (Figure 6(C)).

The background (resting) level of MIP-2 production was found to be relatively high in J774A.1 cells (Figure 7). However, the secretion of this protein was shown to be significantly increased in response to numerous materials, including CMS-*f/h*, CMS-*f*, MS-*f/h*, CaS-*f* and CaS-*f/h*, but not in response to MS-*f* or either RCF. Both TiO₂ and DQ12 caused a significant increase in MIP-2 secretion. DQ12 was substantially more reactive than the other materials, with an approximate 10 fold greater response observed (Figure 7(C)).

Statistical analysis to compare heat-treated HTIW containing crystalline silica with unheated HTIW established that heated MS-*f/h* induced significantly greater GRO- α release than the unheated MS-*f* (Figure 4), while the heated CMS-*f/h* induced significantly more RANTES and MIP-2 than the unheated CMS-*f* (Figures 6 and 7).

For the control treatments, the LPS positive control induced the secretion of all mediators measured from J774A.1 cells. In addition to the results described above, DQ12 also induced significant secretion of all cytokines, except GM-CSF and IL-1 β .

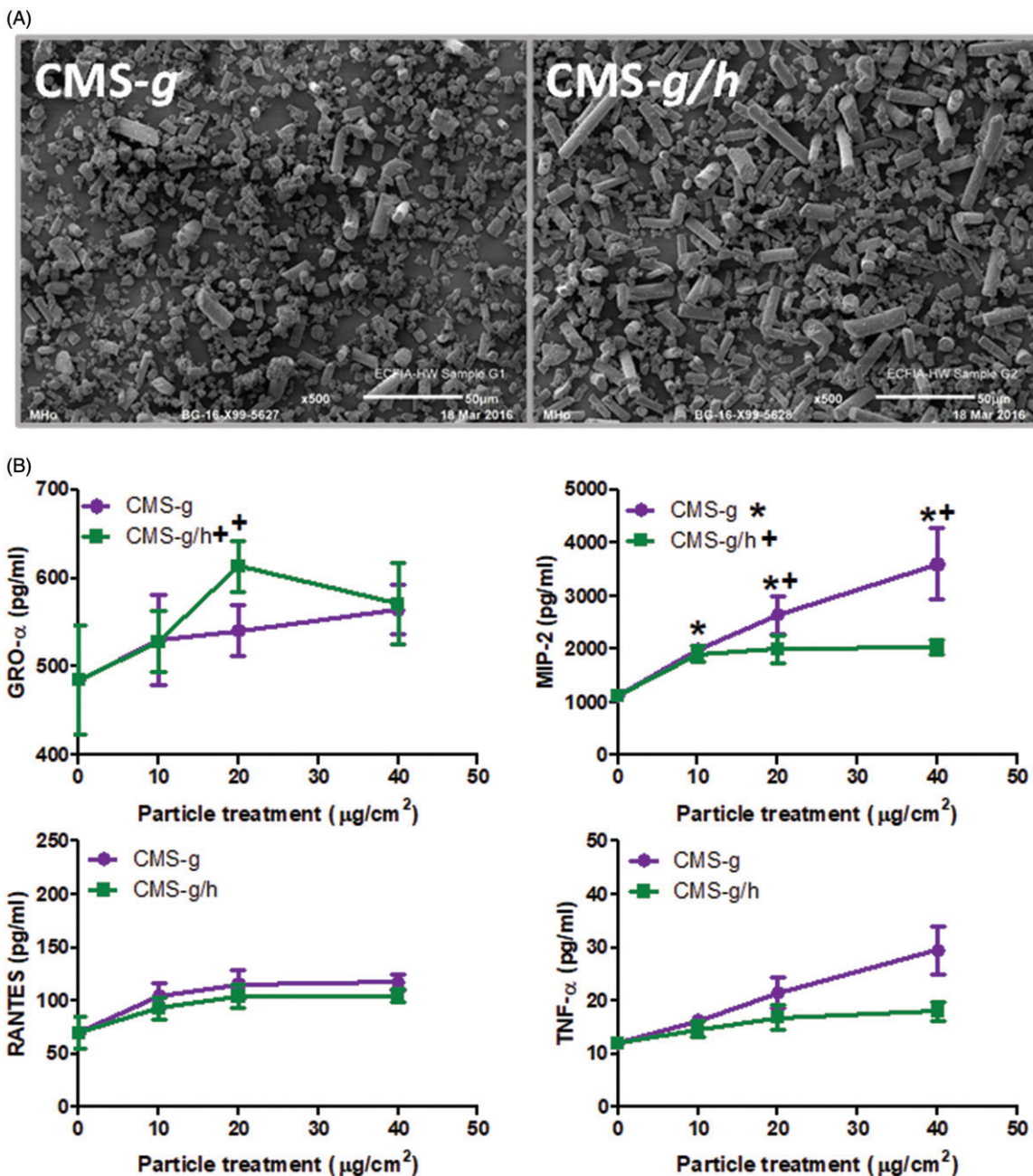


Figure 9. (A) Scanning electron microscopy images of calcium magnesium silicate wools investigated after the fibers had been ground to create a less fibrous morphology, including CMS-g (unheated) and CMS-g/h (heated). The scale of each image is included at the bottom right of each image, and represents 50 μm . (B) GRO- α release from A549 cells and MIP-2, RANTES and TNF- α release from J774A.1 cells, all treatments were for 24 h with 0–40 $\mu\text{g}/\text{cm}^2$ heated and unheated CMS-g. Each data point represents the mean \pm SD of at least three independent biological replicates. Statistical significance of particle exposures in comparison to medium only is indicated when $p < 0.05$, with * for CMS-g and + for CMS-g/h.

Reactive oxygen species generation – acellular

No acellular ROS production, was observed in response to any of the HTIW, when assessed in the presence or absence of FCS, using particle concentrations equivalent to those used for cytokine and chemokine assessment (0–40 $\mu\text{g}/\text{cm}^2$) over a 6-h period (Figure S4). In contrast, DQ12 caused a concentration-dependent increase in ROS formation, which was statistically significant at the highest concentration when the suspension medium contained FCS, and at concentrations $>20 \mu\text{g}/\text{cm}^2$ when FCS was absent. The highest ROS production was observed in response to the positive

controls NPCB and t-BHP (Figure S5). As expected, the negative control TiO_2 did not induce ROS production.

Free radical generation in an acellular system was also assessed using EPR with the Tempone-H (a superoxide free radical-selective spin trap). Of the HTIW, only MS-f caused oxidation of the Tempone-H spin trap, which was shown to be significantly greater (approximately 4-fold) than both the vehicle control and its heated counterpart MS-f/h (Figure S6). Neither DQ12 nor TiO_2 caused spin trap oxidation. Both pyrogallol and NPCB produced a substantial EPR spectrum intensity (Figure S6).

Reactive oxygen species generation – cellular

None of the HTIW samples were found to induce intracellular ROS production, using DCF fluorescence, in either cell line, at any of the concentrations and time points tested (Figure S7). In contrast, DQ12 increased DCFH oxidation in both cell lines in a concentration-dependent manner (Figure S8), with statistical significance reached after a 12-h exposure of J774A.1 cells to the highest particle concentration (Figure S8.D). The positive control NPCB induced the greatest increase (60-fold) in DCFH oxidation with J774A.1 cells (Figure S9), while TiO₂ had no measurable effect (Figure S8).

Aluminum lactate coating and its effect on pro-inflammatory responses

For the assessment of whether an AL coating could lower the inflammatory response of crystalline silica containing materials, all particles and fibers that had previously been shown to induce cytokine production were tested again after coating with AL. Control treatments for these assays used material that had undergone the same coating/washing protocol in the absence of AL.

The DQ12-induced release of GRO- α by A549 cells, and TNF- α and MIP-2 by J774A.1 cells were all significantly lowered when DQ12 was coated with AL (Figure S10). RANTES secretion did not follow this trend, with the AL coating having no impact on RANTES production.

The reduced secretion of GRO- α , TNF- α and MIP-2 in response to AL-coated DQ12 suggests these mediators are produced in response to crystalline silica exposure (Figure S10). These pro-inflammatory mediators were therefore assessed in response to the relevant HTIW (which were previously shown to cause a significant release of these specific cytokines). The following mediators and particles were investigated: GRO- α in response to CMS-*f*, CMS-*f/h*, MS-*f/h*; TNF- α in response to CMS-*f/h* and CaS-*f*; and MIP-2 in response to TiO₂, CMS-*f*, CMS-*f/h*, MS-*f/h*, CaS-*f*, CaS-*f/h*.

The significant increase in release of GRO- α observed in response to CMS-*f/h* by A549 cells, and TNF- α and MIP-2 by J774A.1 cells, was no longer statistically significant compared to the control when this fiber was coated with AL. In addition, the coating of CMS-*f/h* with AL significantly lowered the secretion of GRO- α from A549 cells compared to the uncoated CMS-*f/h* (Figure 8). In contrast CMS-*f* induced a significant release of MIP-2 which was not altered by AL (Figure S11). No secretion of GRO- α was evident in response to the unheated CMS-*f* whether AL was present or not (Figure S11).

With regards to the other materials tested, GRO- α released in response to MS-*f/h* was statistically significant regardless of whether AL was present or not. Furthermore, the previously identified cytokine release in response to CaS-*f* and TiO₂ was no longer observed in this second experimental setup; this was believed to be due to the wash procedure employed. The release of MIP-2 in response to MS-*f/h* and CaS-*f/h* was not influenced by AL coating, even though both materials contain crystalline silica (Figure S11).

Effect of fiber length

The most prominent cytokine responses by J774A.1 cells in response to HTIW were obtained with CMS-*f/h*, which consistently gave responses higher than the unheated CMS-*f*. In A549 cells, the result was somewhat similar to the fibrous samples but at a lower level of significance. We used ground material to determine whether the same pattern was seen in the absence of fibrous form (Figure 9). CMS-*g* did not stimulate GRO- α production at a significant level while the heated CMS-*g/h* caused a significant release of GRO- α , but only at a concentration of 20 $\mu\text{g}/\text{cm}^2$. In J774A.1 cells, RANTES and TNF- α did not give statistically significant responses with the ground material. MIP-2 secretion was induced by both CMS-*g* and CMS-*g/h*, with CMS-*g* causing significantly more MIP-2 than CMS-*g/h*. Generally the response of J774A.1 cells to the CMS-*g/h* samples was lower than the response for CMS-*f/h*.

Discussion

The primary aim of this study was to test whether the crystalline silica in after-service (heated) HTIW presents a potential hazard to individuals involved in maintenance or removal of after-service HTIW-containing structures. To address this aim, we have taken four commercially available HTIW and heated them at high temperatures to elicit crystalline silica formation. The samples included three chemically distinct AES fibers and a RCF sample. Acute biological responses to the different HTIW were assessed *in vitro* in human lung epithelial cells and mouse macrophage-like cells. The main findings of this study, including ROS generation, initiation of pro-inflammatory responses, and cell death are represented as a heatmap in Figure S12.

In this study, the RCF sample and all of the HTIW were unable to induce cell death in either the epithelial or macrophage cell lines during the 24 h exposure period, which was in contrast to the detectable cytotoxicity of DQ12. Heating of the RCF and AES did not enhance their cytotoxicity. This suggests that the crystalline silica content of HTIW was either lower in quantity or bioreactivity than that of DQ12. Our results concur with those of Ziemann et al., (2014), who found no LDH release from alveolar macrophages in response to heated and unheated AES fibers exposed for 2 h. The present study showed that both the alveolar epithelial (A549) and macrophage (J774A.1) cell lines were sensitive to DQ12-induced cell death, with a greater sensitivity of macrophages over the epithelial cell line, again corresponding with other studies (Clouter et al., 2001; Nadeau et al., 1996; Schins et al., 2002). The mechanisms and rates of particle internalization between macrophages and epithelial cells differ, with macrophages (including J774A.1) displaying a greater rate of particle uptake than epithelial cells (including A549 cells) (Breznan et al., 2017) as they are professional phagocytes. This relatively higher rate of uptake is likely why the J774A.1 cells were affected to a greater extent than the A549 cells. In this study, assessment of the interaction between the test samples and macrophages was prioritized, as existing studies have

demonstrated that inhaled particles and fibers accumulate primarily in macrophages, and as failure of macrophages to clear inhaled particles and fibers is key to their pathogenicity (via stimulation of frustrated phagocytosis). However future studies would be required to assess the interaction of the test materials with A549 cells.

The cytotoxicity data allowed selection of sublethal concentrations to study biological responses other than cell death. In these subsequent experiments, certain HTIW had the capacity to induce a low-level pro-inflammatory cytokine release *in vitro*. Moreover, these responses allowed some distinction between those fibers that contained crystalline silica and those that did not. For example, the heating of CMS-*f* to CMS-*f/h* increased its capacity to induce the release of pro-inflammatory mediators from macrophages, but not epithelial cells. Out of all the HTIW assessed here, cristobalite-containing CMS-*f/h* induced a higher and more consistent pro-inflammatory response than the other HTIW. However, CMS-*f/h* did not contain the greatest concentration of crystalline silica and the response was not replicated in CMS-*g/h*. Therefore, crystalline silica content is unlikely to be the only influencing factor on CMS-*f/h* toxicity. Similar to CMS-*f*, the heating of MS-*f* to MS-*f/h* also increased pro-inflammatory mediator production, but this time for epithelial cells only. For other HTIW, such as CaS-*f* and RCF-*f*, heating caused no additional cytokine or chemokine secretion. Overall, this suggests that while the cristobalite content may have contributed to the cellular responses to some HTIW (particularly CMS-*f/h*), this was not consistent across the different HTIW samples. In fact, cytokine release was seen to correspond with HTIW samples that possessed both high calcium content and a high solubility, suggesting that the biological responses observed were driven by a combination of these three physicochemical attributes. These general trends are shown in the spider diagrams (Figures S13 and S14), which also identify those characteristics that appeared to have little effect upon cytokine/chemokine release including aluminum content, magnesium content and low solubility.

For some AES, solubility is reported to be far greater at pH 7.4 than at pH 4.5 (Campopiano et al., 2014). In our study, the solubility of HTIW was marginally greater at pH 4.5 than at pH 7.4, suggesting differences between different AES or the protocol used. In general, heating decreased the solubility of the HTIW. Exceptions included CMS-*f/h* and CaS-*f/h*, which retained a higher degree of solubility following heating. CMS-*f/h* retained a high solubility at both pH 4.5 and 7.4, and CaS-*f/h* only at pH 7.4. Taken together, the data obtained in this study support the hypothesis that, for CMS, a combination of crystalline silica and high solubility contributed to a pro-inflammatory response to after-service HTIW. This does not necessarily imply that these effects would translate to deleterious *in vivo* responses, as the increased solubility and lower biopersistence of AES *in vivo* have been attributed to lower toxicity (Bellmann et al., 2002; Bellmann et al., 2010; Bernstein et al., 1996; Brown et al., 2002; Brown & Harrison, 2012; Hesterberg et al., 1998). In addition, the biological relevance of the amplitude of the

cellular responses to AES observed here needs to be considered.

To further discern the contribution of crystalline silica in the observed cytokine/chemokine secretion, we coated the test materials with AL. The impact of AL coating on cytokine release varied depending on fiber chemistry. Mediator release induced by CMS-*f/h* tended to be reduced or removed when coated with AL. In contrast coating either MS-*f/h* or CaS-*f/h* with AL had a negligible effect on cytokine responses. The effects of AL on DQ12-induced responses were clear, with consistent attenuation of cytokine responses in both cell types. These data concur with previous studies using AL-induced attenuation of crystalline silica responses *in vitro* and *in vivo* (Albrecht et al., 2005; Brown et al., 1989; Duffin et al., 2001; Schins et al., 2002; Stone et al., 2004), and provides further support for the role of cristobalite in driving the biological effects induced by CMS-*f/h*.

However, it should be questioned why the patterns in pro-inflammatory mediator release in response to CMS were not observed for all HTIW. Using the techniques employed, it was not possible to determine whether the cristobalite resided at the fiber surface or if it was hidden within the fiber. In fact it has been postulated that the devitrified silica within such materials may not be bioavailable (Harrison & Brown, 2011). It is feasible, that for the materials exhibiting a lower solubility after heating, the cristobalite remained trapped within the fiber, while for the CMS which retained a relatively high solubility, the cristobalite might have been revealed as the surrounding material was dissolved. This hypothesis, however, does not entirely align with the above-mentioned AL-attenuated effects. As the AL was used as a pre-coating method, any cristobalite revealed through dissolution of soluble components might still become bioavailable, making it unclear as to how AL pre-coating reduced its effects. One explanation may be that the AL could have hindered fiber dissolution, therefore blocking both surface-orientated cristobalite as well as preventing further revealing of cristobalite positioned within the fibers. However, this was not tested. Alternatively, the ultra-sonication (used to separate the sintered material formed upon heating) may have induced cleavage points on fiber surfaces, exposing crystalline silica. Since the cristobalite-attributed effects were only observed for CMS, this hypothesis may reflect the instability of the heated CMS material, which was also evident in the retained solubility following heating. A further explanation may be that the aluminum oxide within certain fibers modified the ability of HTIW to induce biological effects. By incorporating small amounts (1.4 wt% and above) of Al₂O₃ during the formation of cristobalite, Natrass et al., (2017) were able to reduce the amount of cristobalite-induced cell death in J774A.1 macrophages. In the present study CMS was the only material containing Al₂O₃ at a concentration lower than that used by Natrass et al., (2017), and so it is possible that the cristobalite formed in CMS-*f/h* had fewer impurities within its structure compared to the other HTIW tested here.

In parallel, we also evaluated the biological activity of ground forms of CMS to explore the role of fiber length in these responses. In general, the cytokine/chemokine release generated by the ground material was less than that generated by the fibrous material, except for the release of MIP-2. This seems to indicate the importance of a fibrous form for most of the observed responses to CMS-*f/h*. The unheated ground CMS-*g* caused similar levels of MIP-2 secretion as the heated fibrous CMS-*f/h*. Moreover, for MIP-2, the response of CMS-*g* was stronger than that of CMS-*g/h*. CMS-*g* did not contain crystalline silica, which implies that another causative factor was involved. CMS-*g* had a high surface area, and it should be noted that an increase in surface area has been linked to the presence of a significant fraction of particularly small particles (Wittmaack, 2007). However, the solubility data for CMS did not fully support the theory that the ground material had a substantially greater surface area than the fibrous material; a full explanation further testing would be required.

Of the HTIW tested in the study, the lack of response to RCF may at first appear surprising, as these *in vitro* data conflict with the data from past *in vivo* studies. However, this may be explained by differences in interpreting *in vitro* and *in vivo* studies, especially when evaluating fibers. While *in vitro* toxicity tests are useful in identifying mechanistic pathways which may lead to fiber pathogenicity (Bernstein et al., 2005), the intrinsic short-term nature of *in vitro* studies mean they cannot adequately address longer-term effects such as the role of biopersistence in fiber pathology (IARC, 2002). In fact, it is only with longer lung retention times that the soluble fibers decrease in size and concomitantly in toxicity, while persistent fibers persist to induce pathology (IARC 2002). However, the biological responses that were generated by HTIW in this *in vitro* study were low compared to DQ12. Due to its pathogenic behavior, DQ12 has often been used as a standard experimental quartz sample (Berube et al., 2009; Clouter et al., 2001). A strong pro-inflammatory cytokine response to DQ12 was observed in the present study, which aligns well with much of the existing *in vitro* literature (Bauer et al., 2012; Driscoll et al., 1996; Nattrass et al., 2015; Øvrevik et al., 2008; Westphal et al., 2015). Since the cytokine response to HTIW was considerably less than to DQ12, the biological significance of the HTIW induced cytokine/chemokine release observed needs to be considered since statistical significance does not always mean biological significance.

In our study, the statistically significant release of TNF- α induced by all HTIW was lower than 100 pg/mL, while responses to DQ12 were in the range of 100–1000 pg/mL. An *in vitro* chemotaxis model used by McCourt et al., (1999) required TNF- α at concentrations of at least 2.5 ng/mL to cause the stimulation of neutrophil chemotaxis, suggesting the concentrations generated by HTIW might have been too low to induce such a chemotactic response. Also using an *in vitro* model of chemotaxis, neutrophil chemotaxis was observed in response to 10 ng/mL GRO- α (De Filippo et al., 2013). This is approximately the concentration of GRO- α reached in response to the DQ12 in the present

study, while any significant releases of GRO- α in response to the CMS or MS were an order of magnitude lower. Elsewhere, the migration of neutrophils *in vitro* has been shown in response to approximately 8 ng/mL MIP-2, and *in vivo* a localized exposure to 80 ng/mL MIP-2 (in transplanted matrigel) was shown to encourage neutrophil recruitment (Scapini et al., 2004). In the present study, the CMS-*f/h* induced the release of approximately 3 ng/mL more MIP-2 than the untreated cells over a 24 h period, and the response to DQ12 was again an order of magnitude greater than any HTIW response (\sim 30 ng/mL MIP-2). Overall, this data suggests that such small statistically significant changes in cytokine expression are not likely to evoke an inflammatory response for the unheated and heated HTIW. This hypothesis would require more work to confirm or refute. However, there is no evidence that the cristobalite content of heated HTIW per se is a strong and consistent predictor of increased biological activity over and above that of the unheated HTIW.

It is worth noting that as the samples we have used were produced from standard production samples, and represent potential workplace dust. However, this does not guarantee that all would be respirable. Fibers of 50 μ m or greater in length have the potential to reach beyond the ciliated airways (Donaldson et al., 2013), and by the World Health Organization (WHO) definition, a fiber must have an aspect ratio of over 3:1, with a length greater than 5 μ m and a diameter under 3 μ m, to allow respirability (WHO, 1997). Although WHO use a conservative length of 5 μ m for fibers, the literature suggests that lengths of over 15 μ m prevent clearance from the lung due to an inability of cells to take up the fibers leading to frustrated phagocytosis (Donaldson et al., 2010; Hamilton et al., 2009). All of the fibers tested here were shown to be of a dimension which might elicit frustrated phagocytosis. SEM imaging supported the hypothesis of frustrated phagocytosis, but as discussed above this was not associated with increased ROS and cytokine production, perhaps due to the solubility of the HTIW. Such an effect has the potential to lead to the sustained release of pro-inflammatory mediators and generation of ROS (Boyles et al., 2015). In this study, the aspect ratio of all fibers was greater than 3:1, the average fiber lengths were greater than 15 μ m, and although the average diameter was below 3 μ m for only CMS-*f* all fibers had a large proportion below 3 μ m. The proportion of each sample determined to be respirable was found to be variable, from 25% of CaS-*f/h* up to 60% of CMS-*f*.

Conclusions

The present study investigated the biological response to unheated and heat-treated HTIW *in vitro* in order to better understand the role of cristobalite, if any, in driving cellular responses. The study was designed to inform upon the potential hazard of after-service HTIW to workers during dismantling of structures such as a furnace. With determination of acellular and intracellular ROS generation, cytotoxicity, and pro-inflammatory mediator release from epithelial

and macrophage cell lines, we have demonstrated that any responses to HTIW are orders of magnitudes lower than the Class 1 carcinogen α -quartz. While there was clear evidence that heating led to devitrification and the formation of cristobalite in all of the HTIW chemistry types, this study demonstrated that this did not necessarily increase biological activity, and that cristobalite content alone was not sufficient in explaining the materials' low but significant pro-inflammatory responses *in vitro*, instead this appears to involve a combination of cristobalite content, solubility, calcium content and fiber dimension.

Disclosure statement

Two authors of this manuscript, JK and MH, are employed by Morgan Advanced Materials, which is one of the companies represented by ECFIA. JK and MH were responsible for preparation of the HTIW used in this study. The authors declare that there are no other conflicts of interest.

Funding

The authors kindly thank ECFIA (an association representing the high temperature insulation wool industry) for the funding this study; MRM is funded by a British Heart Foundation Special Project Grant [SP/15/8/31575].

ORCID

Mark R. Miller  <http://orcid.org/0000-0002-7078-597X>

References

- Albrecht C, Knaapen AM, Becker A, et al., (2005). The crucial role of particle surface reactivity in respirable quartz-induced reactive oxygen/nitrogen species formation and APE/Ref-1 induction in rat lung. *Resp Res* 6:129.
- Alexander IC, Brown RC, Jubb GA, et al., (1994). Durability of ceramic and novel man-made mineral fibers. *Environ Health Pers* 102: 67–71.
- Appay V, Rowland-Jones SL. (2001). RANTES: a versatile and controversial chemokine. *Trends Immunol* 22:83–7.
- Barlow PG, Clouter-Baker A, Donaldson K, et al., 2005. Carbon black nanoparticles induce type II epithelial cells to release chemotaxins for alveolar macrophages. *Particle Fibre Toxicol.* 2:11.
- Bauer M, Gräbsch C, Gminski R, et al., (2012). Cement-related particles interact with proinflammatory IL-8 chemokine from human primary oropharyngeal mucosa cells and human epithelial lung cancer cell line A549. *Environ Toxicol* 27:297–306.
- Bellmann B, Muhle H, Pohlmann G, et al., (2002). Subchronic studies on man-made vitreous fibres: kinetics of inhaled particles. *Ann Occup Hygiene* 46:166–9.
- Bellmann B, Schaeffer HA, Muhle H. (2010). Impact of variations in the chemical composition of vitreous mineral fibers on biopersistence in rat lungs and consequences for regulation. *Inhal Toxicol* 22:817–27.
- Bernstein D, Castranova V, Donaldson K, et al., (2005). Testing of fibrous particles: short-term assays and strategies. *Inhal Toxicol* 7: 497–537.
- Bernstein D, Morscheidt C, Grimm H-G, et al., (1996). Evaluation of soluble fibers using the inhalation biopersistence model, a nine-fiber comparison. *Inhalat Toxicol* 8:345–85.
- BeruBe K, Aufderheide M, Breheny D, et al., 2009. In vitro models of inhalation toxicity and disease. The report of a FRAME workshop. *Alternatives to laboratory animals: ATLA.* 37:89–141.
- Boffetta P, Donaldson K, Moolgavkar S, Mandel J. (2014). A systematic review of occupational exposure to synthetic vitreous fibers and mesothelioma. *Crit Rev Toxicol* 44:436–49.
- Borm PJA, Tran L, Donaldson K. (2011). The carcinogenic action of crystalline silica: a review of the evidence supporting secondary inflammation-driven genotoxicity as a principal mechanism. *Crit Rev Toxicol* 41:756–70.
- Boyles MSP, Young L, Brown DM, et al., (2015). Multi-walled carbon nanotube induced frustrated phagocytosis, cytotoxicity and pro-inflammatory conditions in macrophages are length dependent and greater than that of asbestos. *Toxicol In Vitro* 29:1513–28.
- Breznan D, Das DD, O'Brien JS, et al., (2017). Differential cytotoxic and inflammatory potency of amorphous silicon dioxide nanoparticles of similar size in multiple cell lines. *Nanotoxicology* 11: 223–35.
- Brody AR, Roe MW, Evans JN, Davis GS. (1982). Deposition and translocation of inhaled silica in rats. Quantification of particle distribution, macrophage participation, and function. *Laboratory investigation. J Tech Methods Pathol* 7:533–42.
- Brown RC, Bellmann B, Muhle H, et al., (2002). Subchronic studies on man-made vitreous fibres: toxicity results. *Ann Occup Hygiene* 46: 102–4.
- Brown GM, Donaldson K, Brown DM. (1989). Bronchoalveolar leukocyte response in experimental silicosis: Modulation by a soluble aluminum compound. *Toxicol Appl Pharmacol* 101:95–105.
- Brown RC, Harrison PTC. (2012). Alkaline earth silicate wools – A new generation of high temperature insulation. *Regul Toxicol Pharmacol* 64:296–304.
- Brown TP, Harrison PTC. (2014). Crystalline silica in heated man-made vitreous fibres: A review. *Regul. Toxicol. Pharmacol* 68:152–9.
- Brown DM, Wilson MR, MacNee W, et al., (2001). Size-dependent proinflammatory effects of ultrafine polystyrene particles: a role for surface area and oxidative stress in the enhanced activity of ultrafines. *Toxicol Appl Pharmacol* 175:191–9.
- Cakmak GD, Schins RP, Shi T, et al., (2004). In vitro genotoxicity assessment of commercial quartz flours in comparison to standard DQ12 quartz. *Int J Hygiene Environ Health* 207:105–13.
- Campopiano A, Cannizzaro A, Angelosanto F, et al., (2014). Dissolution of glass wool, rock wool and alkaline earth silicate wool: morphological and chemical changes in fibers. *Regul Toxicol Pharmacol* 70:393–406.
- Chiazze LJ, Watkins DK, Fryar C. (1997). Historical cohort mortality study of a continuous filament fiberglass manufacturing plant: I white men. *J Occup Environ Med* 39:432–41.
- Clouter A, Brown D, Höhr D, et al., (2001). Inflammatory effects of respirable quartz collected in workplaces versus standard DQ12 quartz: particle surface correlates. *Toxicol Sci* 63:90–8.
- Comodi P, Cera F, Gatta GD, et al., (2010). The devitrification of artificial fibers: a multimethodic approach to quantify the temperature–time onset of cancerogenic crystalline phases. *Ann Occup Hygiene.* 54:893–903.
- Connolly M, Fernandez-Cruz M-L, Quesada-Garcia A, et al., (2015). Comparative cytotoxicity study of silver nanoparticles (AgNPs) in a variety of rainbow trout cell lines (RTL-W1, RTH-149, RTG-2) and primary hepatocytes. *Int J Environ Res Public Health* 12:5386.
- Cullen RT, Miller BG, Davis JM, et al., (1997). Short-term inhalation and in vitro tests as predictors of fiber pathogenicity. *Environ Health Perspect* 105:1235–40.
- De Filippo K, Dudeck A, Hasenberg M, et al., (2013). Mast cell and macrophage chemokines CXCL1/CXCL2 control the early stage of neutrophil recruitment during tissue inflammation. *Blood* 121: 4930–7.
- Donaldson K, Murphy FA, Duffin R, Poland CA. (2010). Asbestos, carbon nanotubes and the pleural mesothelium: a review of the hypothesis regarding the role of long fibre retention in the parietal pleura, inflammation and mesothelioma. *Particle Fibre Toxicol* 7:5.

- Donaldson K, Poland CA, Murphy FA, et al., (2013). Pulmonary toxicity of carbon nanotubes and asbestos — Similarities and differences. *Adv Drug Deliv Rev* 65:2078–86.
- Driscoll KE. (2000). TNF α and MIP-2: role in particle-induced inflammation and regulation by oxidative stress. *Toxicol Lett* 112–113: 177–83.
- Driscoll KE, Carter JM, Hassenbein DG, Howard B. (1997). Cytokines and particle-induced inflammatory cell recruitment. *Environ Health Perspect* 105:1159–64.
- Driscoll KE, Howard BW, Carter JM, et al., (1996). Alpha-quartz-induced chemokine expression by rat lung epithelial cells: effects of in vivo and in vitro particle exposure. *Am J Pathol* 149:1627–37.
- Duffin R, Gilmour PS, Schins RPF, et al., (2001). Aluminium lactate treatment of DQ12 quartz inhibits its ability to cause inflammation, chemokine expression, and nuclear factor- κ B activation. *Toxicol Appl Pharmacol* 176:10–17.
- Dutta D, Moudgil BM. (2007). Crystalline silica particles mediated lung injury. *KONA Powder Particle J* 25:76–87.
- ECFIA. 2014. Crystalline silica in High Temperature Insulation Wool (HTIW) products after use in high temperature applications. Available from: http://www.ecfiaeu/files/ECFIA-Action-Crystalline_Silica-v2_0-2014-10.pdf [Accessed 13 November 2017].
- Ernst H, Rittinghausen S, Bartsch W, et al., (2002). Pulmonary inflammation in rats after intratracheal instillation of quartz, amorphous SiO₂, carbon black, and coal dust and the influence of poly-2-vinylpyridine-N-oxide (PVNO). *Exp Toxicol Pathol* 54:109–26.
- Fanizza C, Ursini CL, Paba E, et al., (2007). Cytotoxicity and DNA-damage in human lung epithelial cells exposed to respirable alpha-quartz. *Toxicol In Vitro Int J* 21:586–94.
- Foucaud L, Wilson MR, Brown DM, Stone V. (2007). Measurement of reactive species production by nanoparticles prepared in biologically relevant media. *Toxicol Lett* 74:1–9.
- Gamble JL. 1967. Chemical anatomy, physiology and pathology of extracellular fluid: a lecture syllabus. Cambridge, MA: Harvard University Press.
- Ganz R, Krönert W. (1982). Crystallisation behaviour of high temperature ceramic fibres of the Al₂O₃-SiO₂ system. *Interceram* 31: 136–44.
- Geiser M, Casaulta M, Kupferschmid B, et al., (2008). The role of macrophages in the clearance of inhaled ultrafine titanium dioxide particles. *Am J Resp Cell Molecul Biol* 38:371–6.
- Guha N, Straif K, Benbrahim-Tallaa L. (2011). The IARC monographs on the carcinogenicity of crystalline silica. *Med Lav* 2:310–20.
- Hamilton RF, Wu N, Porter D, et al., (2009). Particle length-dependent titanium dioxide nanomaterials toxicity and bioactivity. *Particle Fibre Toxicol* 6:35.
- Harrison PTC, Brown RC. (2011). Devitrification of artificial fibres. *Ann Occup Hyg* 55:823–4.
- Hart GA, Newman MM, Bunn WB, Hesterberg TW. (1992). Cytotoxicity of refractory ceramic fibres to Chinese hamster ovary cells in culture. *Toxicol In Vitro* 6:317–26.
- Hesterberg TW, Hart GA, Chevalier J, et al., (1998). The importance of fiber biopersistence and lung dose in determining the chronic inhalation effects of X607, RCF1, and chrysotile asbestos in rats. *Toxicol Appl Pharmacol* 53:68–82.
- Hefland RB, Schwarzel PE, Johansen BV, et al., (2001). Silica-induced cytokine release from A549 cells: importance of surface area versus size. *Human Experi Toxicol* 20:46–55.
- IARC IAfRoC. 2002. Monographs on the Evaluation of Carcinogenic Risks to Humans. Man-made Vitreous Fibers. vol. 81.
- IARC IAfRoC 2012. Monographs on the Evaluation of Carcinogenic Risks to Humans. Arsenic, Metals, Fibres and Dusts. vol. 100C.
- Kokubo T, Ito S, Shigematsu M, et al., (1987). Fatigue and life-time of bioactive glass-ceramic A-W containing apatite and wollastonite. *J Mater Sci* 22:4067–70.
- Kolling A, Ernst H, Rittinghausen S, Heinrich U. (2011). Relationship of pulmonary toxicity and carcinogenicity of fine and ultrafine granular dusts in a rat bioassay. *Inhalation Toxicol* 23:544–54.
- Kreyling WG. (1992). Intracellular particle dissolution in alveolar macrophages. *Environ Health Perspect* 97:121–6.
- Lasfargues G, Lison D, Maldague P, Lauwerys R. (1992). Comparative study of the acute lung toxicity of pure cobalt powder and cobalt-tungsten carbide mixture in rat. *Toxicol Appl Pharmacol* 112:41–50.
- Lieber M, Todaro G, Smith B, et al., (1976). A continuous tumor-cell line from a human lung carcinoma with properties of type II alveolar epithelial cells. *Int J Cancer* 17:62–70.
- Luoto K, Holopainen M, Sarataho M, Savolainen K. (1997). Comparison of cytotoxicity of man-made vitreous fibres. *Ann Occup Hyg* 41:37–50.
- Maciejewska A. (2014). Health effects of occupational exposure to crystalline silica in the light of current research results. *Med Pr* 65: 799–818.
- Marques MRC, Loebenberg R, Almukainzi M. (2011). Simulated biological fluids with possible application in dissolution testing. *Dissolution Technol* 18:15–28.
- Mast RW, McConnell EE, Anderson R, et al., (1995). Studies on the chronic toxicity (inhalation) of four types of refractory ceramic fiber in male Fischer 344 rats. *Inhal Toxicol* 7:425–67.
- McCourt M, Wang J, Sookhai S, Redmond H. (1999). Proinflammatory mediators stimulate neutrophil-directed angiogenesis. *Arch Surg* 134:1325–31.
- Meißner T, Kühnel D, Busch W, et al., (2010). Physical-chemical characterization of tungsten carbide nanoparticles as a basis for toxicological investigations. *Nanotoxicology* 4:196–206.
- Miller MR, Borthwick SJ, Shaw CA, et al., (2009). Direct impairment of vascular function by diesel exhaust particulate through reduced bioavailability of endothelium-derived nitric oxide induced by superoxide free radicals. *Environ Health Perspect* 7:611–6.
- Monteiller C, Tran L, MacNee W, et al., (2007). The pro-inflammatory effects of low-toxicity low-solubility particles, nanoparticles and fine particles, on epithelial cells in vitro: the role of surface area. *Occup Environ Med* 64:609–15.
- Mossman BT, Glenn RE. (2013). Bioreactivity of the crystalline silica polymorphs, quartz and cristobalite, and implications for occupational exposure limits (OELs). *Crit Rev Toxicol* 43:632–60.
- Nadeau D, Vincent R, Kumarathasan P, et al., (1996). Cytotoxicity of ambient air particles to rat lung macrophages: Comparison of cellular and functional assays. *Toxicol In Vitro* 10:161–72.
- Naha PC, Davoren M, Lyng FM, Byrne HJ. (2010). Reactive oxygen species (ROS) induced cytokine production and cytotoxicity of PAMAM dendrimers in J774A.1 cells. *Toxicol Appl Pharmacol* 246: 91–9.
- Natras C, Horwell CJ, Damby DE, et al., (2017). The effect of aluminium and sodium impurities on the in vitro toxicity and pro-inflammatory potential of cristobalite. *Environ Res* 159:164–75.
- Natras C, Horwell CJ, Damby DE, et al., (2015). The global variability of diatomaceous earth toxicity: a physicochemical and in vitro investigation. *J Occup Med Toxicol* 10:23.
- Nel A, Xia T, Mädler L, Li N. (2006). Toxic potential of materials at the nanolevel. *Science* 311:622–7.
- Oberdörster G. (2002). Toxicokinetics and effects of fibrous and nonfibrous particles. *Inhal Toxicol* 14:29–56.
- Oberdörster G, Castranova V, Asgharian B, Sayre P. (2015). Inhalation exposure to carbon nanotubes (CNT) and carbon nanofibers (CNF): methodology and dosimetry. *J Toxicol Environ Health, Part B* 8: 121–212.
- Osmond-McLeod MJ, Poland CA, Murphy F, et al., (2011). Durability and inflammatory impact of carbon nanotubes compared with asbestos fibres. *Particle Fibre Toxicol* 8:15.
- Ovrevik J, Refsnes M, Schwarze P, Lag M. (2008). The ability of oxidative stress to mimic quartz-induced chemokine responses is lung cell line-dependent. *Toxicol Lett* 181:75–80.
- Pang C, Neubauer N, Boyles M, et al., (2017). Releases from transparent blue automobile coatings containing nanoscale copper phthalocyanine and their effects on J774 A1 macrophages. *NanoImpact* 7: 75–83.
- Piret J-P, Bondarenko OM, Boyles MSP, et al., (2017). Pan-European inter-laboratory studies on a panel of in vitro cytotoxicity and pro-inflammation assays for nanoparticles. *Arch Toxicol* 91:2315–30.

- Porter DW, Ramsey D, Hubbs AF, et al., (2001). Time course of pulmonary response of rats to inhalation of crystalline silica: histological results and biochemical indices of damage, lipidosis, and fibrosis. *J Environ Pathol Toxicol Oncol* 20: 14.
- Renwick LC, Brown D, Clouter A, Donaldson K. (2004). Increased inflammation and altered macrophage chemotactic responses caused by two ultrafine particle types. *Occup Environ Med.* 61:442–7.
- Rothen-Rutishauser B, Brown DM, Piallier-Boyles M, et al., (2010). Relating the physicochemical characteristics and dispersion of multiwalled carbon nanotubes in different suspension media to their oxidative reactivity in vitro and inflammation in vivo. *Nanotoxicology* 4:331–42.
- Sawyer RT, Moon RJ, Beneke ES. (1981). Trapping and killing of candida albicans by corynebacterium parvum-activated livers. *Infect Immun.* 32:945–50.
- Scapini P, Morini M, Tecchio C, et al., (2004). CXCL1/macrophage inflammatory protein-2-induced angiogenesis in vivo is mediated by neutrophil-derived vascular endothelial growth factor-A. *J Immunol* 172:5034–40.
- Schins RPF, Duffin R, Höhr D, et al., (2002). Surface modification of quartz inhibits toxicity, particle uptake, and oxidative DNA damage in human lung epithelial cells. *Chem Res Toxicol.* 15:1166–73.
- Schlinkert P, Casals E, Boyles M, et al., (2015). The oxidative potential of differently charged silver and gold nanoparticles on three human lung epithelial cell types. *J Nanobiotechnol* 13:1.
- Smith DF, Galkina E, Ley K, Huo Y. (2005). GRO family chemokines are specialized for monocyte arrest from flow. *Am J Physiol* 289: H1976–84.
- Stone V, Jones R, Rollo K, et al., (2004). Effect of coal mine dust and clay extracts on the biological activity of the quartz surface. *Toxicol Lett* 149:255–9.
- Tomatis M, Fenoglio I, Elias Z, et al., (2002). Effect of thermal treatment of refractory ceramic fibres on the induction of cytotoxicity and cell transformation. *Ann Occup Hygiene* 46:176–80.
- Tomlinson GS, Booth H, Petit SJ, et al., (2012). Adherent human alveolar macrophages exhibit a transient pro-inflammatory profile that confounds responses to innate immune stimulation. *PLoS One* 7:e40348.
- van Ravenzwaay B, Landsiedel R, Fabian E, et al., (2009). Comparing fate and effects of three particles of different surface properties: Nano-TiO₂, pigmentary TiO₂ and quartz. *Toxicol Lett* 186:152–9.
- Walker AM, Maxim LD, Utell M. (2002). Risk analysis for mortality from respiratory tumors in a cohort of refractory ceramic fiber workers. *Regul Toxicol Pharmacol* 35:95–104.
- Westphal GA, Schremmer I, Rostek A, et al., (2015). Particle-induced cell migration assay (PICMA): a new in vitro assay for inflammatory particle effects based on permanent cell lines. *Toxicol In Vitro* 29: 997–1005.
- WHO. 1997. World Health Organization. Determination of Airborne Fibre Number Concentrations: A Recommended Method by Phase Contrast Optical Microscopy. World Health Organization, Geneva.
- Wittmaack K. (2006). In search of the most relevant parameter for quantifying lung inflammatory response to nanoparticle exposure: particle number, surface area, or what? *Environ Health Perspect.* 115:187–94.
- Ziemann C, Harrison PTC, Bellmann B, et al., (2014). Lack of marked cyto- and genotoxicity of cristobalite in devitrified (heated) alkaline earth silicate wools in short-term assays with cultured primary rat alveolar macrophages. *Inhal Toxicol* 26:113–27.